

Catalog of Proper Orbits for 1.25 Million Main Belt Asteroids and Discovery of 136 New Collisional Families

David Nesvorný¹, Fernando Roig², David Vokrouhlický³, Miroslav Brož³

(1) *Department of Space Studies, Southwest Research Institute, 1050 Walnut St., Suite 300, Boulder, CO 80302, USA*

(2) *Observatório Nacional, Rua Gal. Jose Cristino 77, Rio de Janeiro, RJ 20921-400, Brazil*

(3) *Institute of Astronomy, Charles University, V Holešovičkách 2, CZ-18000 Prague 8, Czech Republic*

ABSTRACT

The proper elements of asteroids are obtained from the instantaneous orbital elements by removing periodic oscillations produced by gravitational interactions with planets. They are unchanging in time, at least if chaotic dynamics and non-gravitational forces could be ignored, and can therefore be used to identify fragments of major collisions (asteroid families) that happened eons ago. Here we present a new catalog of proper elements for 1.25×10^6 main belt asteroids. We explain the methodology, evaluate uncertainties, and discuss how the new catalog can be used to identify asteroid families. A systematic search for families yielded 153 cases not reported in Nesvorný et al. (2015) – 17 of these cases were identified in various other publications, 136 cases are new discoveries. There are now 274 families in the asteroid belt in total (plus a handful of families in the resonant Hilda population). We analyzed several compact families in detail. The new family around the middle belt asteroid (9332) 1990SB1 (9 members) is the youngest family found so far (estimated formation only 16-17 kyr ago). New families (1217) Maximiliana, (6084) Bascom, (10164) Akusekijima and (70208) 1999RX33 all formed 0.5-2.5 Myr ago. The (2110) Moore-Sitterly family is a close pair of relatively large bodies, 2110 and 44612, and 15 small members all located sunwards from 2110 and 44612, presumably a consequence of the Yarkovsky drift over the estimated family age (1.2-1.5 Myr). A systematic characterization of the new asteroid families is left for future work.

1. Introduction

The orbital elements of asteroids change with time due to gravitational perturbations of planets and other major bodies (e.g. Ceres). The changes can be periodic (i.e., oscillatory) or aperiodic (e.g., chaotic diffusion), and can happen on different timescales. The proper elements are computed from normal (osculating) orbital elements by removing the oscillatory terms. They remain roughly constant on long time intervals, which is useful for studies of asteroid families (e.g., Zappalà et al. 1990, 1994; Parker et al. 2008; Milani et al. 2014; Nesvorný et al. 2015; Novaković et al. 2022). Sophisticated analytic methods were traditionally employed to this purpose (Milani & Knežević 1994), but the ever increasing computer power now allows the proper elements to be computed to a greater precision numerically (Šidlichovský & Nesvorný 1996; Knežević & Milani 2000, 2019). The proper element catalog updates at the AstDys node¹ have been discontinued – they are hosted by B. Novaković at the Asteroid Families Portal (AFP; Novaković et al. 2022).²

The three most useful proper elements are: the proper semimajor axis (a_p), the proper eccentricity (e_p), and the proper inclination (i_p). They are close equivalents to their osculating element counterparts in that they define the average size, elongation and tilt of orbits, respectively. Here we use numerical methods (Sect. 2) to compute a_p , e_p and i_p for main-belt asteroids listed in the most recent Minor Planet Center (MPC) catalog. The new catalog of proper orbits is publicly available.³ The methodology described below is scalable to $\sim 10^7$ bodies and can be used to compute proper orbits for the large volume of main-belt asteroids expected to be discovered by the Rubin Observatory in the next decade (see Sect. 5; Schwamb et al. 2023).

¹<https://newton.spacedys.com/astdys/>

²<http://asteroids.matf.bg.ac.rs/fam/>

³At <https://asteroids.on.br/appeal/>, www.boulder.swri.edu/~davidn/Proper24/, and the Planetary Data System (PDS) node, <https://pds.nasa.gov/>

2. Methods

2.1. Proper elements

The orbital elements of main belt asteroids were downloaded from the MPC catalog on February 9, 2024. We selected asteroid orbits with $a > 1.6$ au and the perihelion distance $q > 1.3$ au (to avoid near-Earth asteroids), aphelion distance $Q < 5$ au (to avoid unstable Jupiter-crossing orbits), and $a < 3.8$ au (to avoid Hildas in the 3:2 resonance with Jupiter).⁴ This represents 1,261,151 orbits in total. We do not distinguish between the numbered and unnumbered (single- or multi-opposition) bodies, but the information about the quality of the osculating orbits (the number of oppositions) is propagated to the final catalog. The osculating orbits are given with respect to the J2000 ecliptic reference system and, for the vast majority of cases, at the JD 2460200.5 epoch (a small number of orbits given at different epochs are ignored). The planetary orbits (Mercury to Neptune) were obtained for the same epoch from the DE 441 Ephemerides (Park et al. 2021). We used the center of mass – planet plus its satellites – and the total mass of each system. The gravitational effects of Ceres and other massive asteroids were ignored (see Tsirvoulis & Novaković 2016).⁵ The reference system was rotated to the invariant plane of planets (as defined by the total angular momentum of planetary orbits).

The orbital integrations were performed with the **Swift** integrator (Levison & Duncan 1994; code `swift_rmvs4`), which is an efficient implementation of the Wisdom-Holman map (Wisdom & Holman 1991). We used a short time step (1.1 days) and integrated all orbits backward in time for 10 Myr.⁶ The backward integration is useful to identify any past

⁴A different strategy must be employed to compute the proper elements for Hildas (Brož & Vokrouhlický 2008, Brož et al. 2011).

⁵We also performed the analysis with Ceres being included as a massive body in the orbital integrations. As the computed proper elements do not show any significant differences, here we report the results for the case without the gravitational effects of Ceres.

⁶We tested different timesteps. The one that was selected for the main integrations is conservatively short. We checked that the integrated orbit of Mercury is stable and does not show any unusual behavior. The semimajor axis of Mercury shows oscillations around a fixed value (i.e., no diffusion) and Mercury’s eccentricity/inclination evolution closely follows expectations. The proper frequencies of Mercury are correctly recovered from the integration. We also recalculated the proper elements of the first 1000 asteroids from an integration where we halved the time step and found that the proper elements and their errors were

convergence of angles, which may indicate the formation time of a young asteroid family (Nesvorný et al. 2002). The symplectic corrector was applied to compensate for high-frequency noise terms (Wisdom 2006). We adopted the general relativistic correction from Quinn et al. (1991). The integrations were split over 12,620 Ivy-bridge cores on the NASA’s Pleiades Supercomputer and ran for 60 wall-clock hours. The orbital elements were saved in double precision every 600 years for the total of 16,666 outputs per orbit.⁷ This allows us to resolve frequencies as high as 1000 arcsec/yr. The binary output files represent 1.3 Tb of data in total. We did not apply any low-pass filter on output, because our previous tests showed that the use of filter did not have an appreciable effect on the final product.

The Frequency Modified Fourier Transform (FMFT; Šidlichovský & Nesvorný 1996, Laskar 1993) was applied to obtain a Fourier decomposition of each signal. We used the complex variable $x(t) + \iota y(t)$ with $x = e \cos(\varpi)$ and $y = e \sin(\varpi)$ for the proper eccentricity, and $x = \sin(i) \cos(\Omega)$ and $y = \sin(i) \sin(\Omega)$ for the proper inclination, where ϖ and Ω are the perihelion and nodal longitudes. FMFT was first applied to the planetary orbits to obtain the planetary frequencies g_j and s_j , governing the perihelion and nodal evolution of planetary orbits, respectively (Table 1). We identified the forced terms with these frequencies in the Fourier decomposition of each asteroid orbit, and subtracted them from asteroid’s $x(t) + \iota y(t)$.

We experimented with different techniques to extract the amplitude of the proper terms from the remaining signal. It is possible, for example, to identify the proper frequency as the largest term in the remaining signal and use FMFT to obtain its amplitude. This is the method recommended in Knežević & Milani (2000). It works perfectly well in the vast majority of cases. For orbits near mean-motion and secular resonances, however, which may be affected by orbital chaos, we observed splitting of the proper term into a number of Fourier terms with similar frequencies. In these cases, the amplitude of the largest proper term usually corresponds to the *minimum* of (e or $\sin(i)$) oscillations, which is inconvenient because the normal proper elements are desired to be close to the *mean* value of osculating elements (Appendix A).

Short Fourier intervals could be used to reduce problems with the proper term splitting,

practically identical to those obtained from the original integration.

⁷We modified the original output scheme in **Swift** such that the fixed output cadence is strictly enforced.

but the optimal interval length is unknown a priori. Also, as long intervals should be used to define more stable proper elements in most cases, one would be tempted to use the Fourier interval that flexibly adjusts from case to case. Unfortunately, according to our tests, it is not obvious how to define robust criteria for the variable interval length.

We therefore opted for a more reliable method which simply consists in computing the mean of $\sqrt{x(t)^2 + y(t)^2}$, with the forced terms removed, over a relatively long interval (2.5 or 5 Myr). We found that the proper elements computed from a longer interval generally have better precision; the 5-Myr window was adopted for the final catalog. This defines the proper elements e_p and $\sin i_p$. Following Knežević & Milani (2000), the proper semimajor axis was computed as the mean value of the osculating semimajor axis over the same time interval. For asteroids in mean-motion resonances, this means that a_p falls near the a value of the exact resonance (e.g., Nesvorný et al. 2002). The uncertainties of a_p , e_p and $\sin i_p$ were obtained as the RMS of the proper elements computed from different intervals within the 10-Myr integration time span.⁸

2.2. Asteroid family identification

We developed several complementary methods to identify asteroid families. The first one consists in visualizing the distribution of proper elements in 3D. Given that no new family is seen to cross the 3:1 ($a = 2.5$ au), 5:2 ($a = 2.825$ au) and 7:3 ($a = 2.958$ au) orbital resonances with Jupiter, we divide the new catalog into four parts: the inner belt ($a < 2.5$ au, including Hungarias), middle belt ($2.5 < a < 2.825$ au), pristine zone ($2.825 < a < 2.958$ au) and outer belt ($2.958 < a < 3.8$ au, excluding Hildas). The search for new families is conducted separately in each of these zones. Two different 3D visualization codes were developed by us (D.N. and M.B.). The first code interactively displays the distribution of proper orbits in a selected zone, allows the user to zoom out and zoom in, and perform any kind of active rotation. The rotation is particularly useful because the user can easily check whether any concentration seen in a projection is a real concentration of proper orbits in

⁸We tested different choices and, for the uncertainties reported in the final catalog, used five equally spaced intervals that cover the whole integration range. Using more intervals slows down the calculation but does not significantly improve the estimate of uncertainties.

3D. The second code displays the $(e_p, \sin i_p)$ projection either in a narrow range of a_p or with the a_p values coded in each dot's color. The dot's size is set inversely proportional to the corresponding object's absolute magnitude which allows the user to identify candidate families that stand out from the background of small and/or large objects.

For each candidate family we identify the lowest numbered asteroid that appears to be associated with the family and use it as the family label. This association is not unique in many cases where there are two or more large bodies in/near the family, with some being more/less offset from the family center. Starting from the labeled bodies we then proceed by identifying each family with the Hierarchical Clustering Method (HCM; Zappalà et al. 1990) and the usual metric

$$d = \frac{3 \times 10^4 \text{ m/s}}{\sqrt{a_p}} \sqrt{\frac{5}{4} (\delta a_p / a_p)^2 + 2(\delta e_p)^2 + 2(\delta \sin i_p)^2}, \quad (1)$$

where $3 \times 10^4 \text{ m/s}$ is the orbital speed at 1 au and δ indicates differences in the proper elements between two neighbor bodies. In each case we test many cutoff distances, d_{cut} , and visualize the results with the interactive software described above.⁹ This allows us to understand how the d_{cut} value needs to be adjusted to identify the whole family seen in 3D. We pay particular attention to the extension of each candidate family in the proper semimajor axis as the orbital resonances can create gaps in the distribution of proper elements and this could artificially divide a family into two or more parts.

D.N. and M.B., working independently, produced two independent lists of candidate families. We then worked together to resolve any differences. The two lists were largely overlapping but there were also $\sim 10\%$ of cases where one of us was more conservative in his approach. We assessed the likelihood that each disputed concentration makes sense from what we know about the formation and dynamical evolution of asteroid families (e.g., Nesvorný et al. 2015). We also used the SDSS colors (Ivezić et al. 2001, Parker et al. 2008) and WISE albedos (Mainzer et al. 2011, Nugent et al. 2015) to check whether identified candidate families are spectroscopically homogeneous, and if so, whether they stand out from colors/albedos of the local background.

⁹HCM clusters bodies by linking them together in a chain where the length of each segment is required to be $d < d_{\text{cut}}$.

The identification method described above is subjective. It uses scientists’ ability to identify concentrations in the 3D distribution of proper elements, and their best judgment to establish whether a perceived concentration does or does not constitute a real asteroid family (i.e. fragments produced by a disruptive collision or spin-up driven fission). We believe that this approach is more powerful and reliable than any of the mathematical and presumably more objective methods proposed elsewhere.¹⁰ For example, the method based on the concept of the so-called Quasi Random Level (QRL; Zappalà et al., 1994) uses the asteroid population in the local background (e.g., in the middle belt) to establish the likelihood that random statistical fluctuations would produce any observed concentration. There are at least two problems with this method. First, the number density in proper element space is highly variable due to the primordial sculpting of the main belt and resonances (e.g., Minton & Malhotra, 2009). Applying the same QRL value in different parts of the main belt can therefore lead to unsatisfactory results (see Nesvorný et al 2015, Section 7.3, for examples). Second, asteroid families do not live in isolation but are frequently close to each other, overlap, and/or are surrounded by empty regions. This introduces an ambiguity in the QRL definition, because it is not clear a priori what region in (a_p, e_p, i_p) space should be considered to define the local QRL in the first place; results depend on this choice.

We used two methods to establish the statistical significance of newly identified candidate families. The first method was proposed in Nesvorný et al. (2002) to demonstrate the high statistical significance of the Karin family, which is embedded in the much larger Koronis family. For that Nesvorný et al. (2002) generated thousand mock orbital distributions corresponding to the Koronis family and applied the HCM to each one. With $d_{\text{cut}} = 10$ m/s, no concentrations in this input were found containing more than a few dozen members, while the Karin family had 541 known members in 2015 (Nesvorný et al. 2015). Therefore, the Karin family is significant at a (much) greater than the 99.9% level. The second method was borrowed from Rozehnal et al. (2016). We created three boxes in the neighborhood of a family, one box centered at the family and the other two boxes below and above the family in $\sin i_p$; the boxes have the same shape and volume in a_p, e_p, i_p . We counted how many asteroids there were in each box, defining N_1 , N_2 and N_3 , where N_2 is the number in the

¹⁰The advantage of mathematical algorithms is that their results are exactly reproducible whereas the ones involving subjective human intervention are not.

middle box containing the candidate family, generated $n = 10^7$ random distributions with $N = N_1 + N_2 + N_3$ bodies in the region covered by all three boxes, and counted the number of positive trials, n^+ , for which the number of randomly generated bodies in the middle box equaled or exceeded N_2 . The probability that the observed number of bodies in the middle box is a result of random fluctuations is then n^+/n , and the statistical significance of the observed family is $1 - n^+/n$. Only families with high statistical significances were included in the final catalog.

3. Catalog

The new catalog of proper elements is available at <https://asteroids.on.br/appeal/>, www.boulder.swri.edu/~davidn/Proper24/, and the PDS node.¹¹ Here we give a brief description of the catalog content. There are 1,249,051 main belt asteroids in total (Fig. 1). Figures 1A-B show the proper orbits from the new catalog. It is clear from these figures that the asteroid belt shows intricate orbital structure (asteroid families, resonances, etc.), which is not obvious from the distribution of osculating elements (Figs. 1C-D). That is, in fact, the chief motivation behind calculating the proper elements: in the proper element space, various orbital structures come into focus (e.g., Milani & Knežević 1994). We do not give proper elements for unstable bodies that were eliminated from the integration in 10 Myr (because they impacted one of the planets, the Sun, or were ejected from the solar system). The ASCII file `eliminated_bodies.dat` lists all eliminated bodies, the time of elimination, and the elimination flag (0 – impact on the Sun, 1 to 8 – planet impacts, 1 is Mercury, 8 is Neptune, 9 - ejection from the solar system).

The proper element catalog (`proper_catalog24.dat`) is an ASCII file with 11 columns. Table 2 shows the first 20 lines of the catalog. The three proper elements are given in columns 1 (a_p), 3 (e_p) and 5 ($\sin i_p$) (columns 2, 4 and 6 list their uncertainties). The proper frequencies g and s are listed in columns 7 and 8 (uncertainties not given for brevity). The absolute magnitudes from MPC are in column 10. Column 11 can be used to select well-

¹¹<https://pds.nasa.gov/>

determined orbits with any number of oppositions.¹² The values given here were imported from the MPC catalog on February 9, 2024 (the source MPC catalog is included in the distribution). The proper element package available on the PDS node also contains the modified `swift_rmvs4` code that was used to integrate orbits and all tools that were used for analysis.¹³

The uncertainties of three proper elements, δa_p , δe_p and $\delta \sin i_p$, can be converted to a single number, d , defined by Eq. (1), where d is the usual metric used for asteroid family identification with HCM (Zappalà et al. 1990). The cumulative distribution of d is shown in Fig. 2. We achieve a slightly better precision than the AFP catalog (Novaković et al. 2022) but the difference is not large. In about 64% of cases the precision is better than 10 m/s, which should be satisfactory for the identification of even very compact families.¹⁴ In about 7% of cases, the error exceeds 100 m/s. Figure 3 shows that this typically happens close to specific mean motion and secular resonances. There are several families with high inclinations (e.g., Hansa, Barcelona) that are affected by these large errors.

In the great majority of cases, however, the precision of the new catalog is good enough to identify known families and recover their intricate dynamical structure. Here we illustrate this on the Veritas family, a well-known family in the outer belt that has been identified as the source of late-Miocene dust shower on the Earth (Farley et al. 2006). Figure 4 compares our proper elements with the AFP catalog (Novaković et al. 2022). The two distributions are very similar. Our catalog has roughly 20% more asteroids than the AFP catalog, which allows some of the subtle features to stand out slightly more clearly. For example, in the left panels of Fig. 4, there are two streaks for $a_p > 3.176$ au, one with slightly higher and one with slightly lower proper eccentricities, that appear to diverge from each other with increasing semimajor axis (these streaks were already visible in the AFP data). The upper

¹²The single-opposition orbits must be used with care. While in most cases the single-opposition orbits are good enough to obtain reliable proper elements, there are also instances where this is not the case. We leave the decision to the user who can easily apply any cut based on the values listed in column 11.

¹³The FMFT code is also available at <https://www.boulder.swri.edu/~davidn/fmft/fmft.html>

¹⁴The HCM cutoff used in the identification of the most compact asteroid families is $d_{\text{cut}} \simeq 10$ m/s. Thus, even the most compact asteroid families can be identified if the precision of proper elements is better than 10 m/s.

streak with $e_p \simeq 0.065\text{--}0.07$ has lower proper inclinations ($\sin i_p \simeq 0.154\text{--}0.158$). This may tell us something interesting about the velocity field of fragments from the site of the original breakup (e.g., Carruba et al. 2016). The vertical features near 3.168 au and 3.174 au are mean motion resonances ((3 3 -2) and (5 -2 -2), respectively; Tsiganis et al. 2007).

4. New asteroid families

Figures 5–8 show the orbital distribution of asteroids in the inner ($a < 2.5$ au), middle ($2.5 < a < 2.825$ au), pristine ($2.825 < a < 2.958$ au) and outer parts ($a > 2.958$ au) of the main belt. We used the methods described in Sect. 2.2 to conduct a search for new asteroid families. All together, we found 153 statistically significant families (see below) that have not been reported in Nesvorný et al. (2015) (Tables 3-7). A cross-check against recent publications revealed that 17 of these families were found previously (Novaković et al. 2011, 2014, 2022; Carruba et al. 2015, 2019; Dykhuis et al. 2015; Novaković & Radović 2019; Tsirvoulis 2019; Brož et al. 2024) and/or are listed in the AFP catalog (Novaković et al. 2022). There are 136 new families: 28 in the inner belt (including Phocaeas)¹⁵, 47 in the middle belt, 15 in the pristine zone, 33 in the outer belt (including Cybeles but excluding Hildas)¹⁶, and 13 with high orbital inclinations ($\sin i_p > 0.3$; Table 7). We used the SDSS colors (Ivezić et al. 2001, Parker et al. 2008) and WISE albedos (Mainzer et al. 2011, Nugent et al. 2015) to determine the taxonomic type of many new families (Tables 3-7).

There were 122 asteroid families reported in Nesvorný et al. (2015). The 153 families identified here therefore represent a 126% increase over the catalog published in Nesvorný et al. (2015). One of the families reported in Nesvorný et al. (2015), (709) Fringilla (FIN 623), was split into two overlapping families, (19093) 1979MM3 and (37981) 1998HD130. There are now 274 known families in the asteroid belt in total (families in the resonant Hilda population are not counted here).

¹⁵There are five new families in Phocaeas: Bezovec, Chesneau, Bascom, 1999 XB232 and 1999 RX33.

¹⁶There is 8 families in Cybeles that were not reported in Nesvorný et al. (2015), 6 with low inclinations ($\sin i_p < 0.3$), Huberta, Liriope, Fukui, Schlichting, 2001 BV20 and 2010 WK8, and 2 with high inclinations ($\sin i_p > 0.3$), Helga and Abastumani. Five of these Cybele families were already identified in Carruba et al. (2015, 2019).

In a great majority of cases, the new families clearly stand out from the background such that their significance is undisputed. We first illustrate the methods described in Sect. 2.2 for the (3787) Aivazovskij (pristine zone) and (4291) Kodaihasu (outer belt) families. These new families are compact but not exceedingly so; they represent a typical case of compact families identified here. (3787) Aivazovskij has 12 members identified with $d_{\text{cut}} = 15$ m/s, (4291) Kodaihasu has 16 members identified with $d_{\text{cut}} = 20$ m/s. Applying the HCM-based method described in Sect. 2.2, we establish that both families are significant at least at the 99.9% level. In the case of (3787) Aivazovskij, there are 12 bodies in the box around the family ($N_2 = 12$), and no bodies in boxes directly below or above ($N = 12$). The probability that this happens by chance is only $\simeq 2.6 \times 10^{-6}$. In the case of (4291) Kodaihasu, there are 16 bodies in the box around the family ($N_2 = 16$), and no bodies in boxes directly below or above ($N = 16$). The probability that this happens by chance is only $\simeq 3 \times 10^{-8}$ (10^8 trials used here). This demonstrates that the two families are statistically significant.

We applied the box method (Sect. 2.2, Rozehnal et al. 2016) to all families identified here. In 137 cases, representing $\simeq 90\%$ of the total of 153, the number of trials (10^7) was insufficient to distinguish the statistical significance from 1. This shows that all these families are significant at least at the 5-sigma level. Table 8 shows the statistical significance for the remaining 16 families. Most of these families are compact and contain a small number of members; these small families are apparently more likely to be produced by statistical fluctuations. Still, in most cases, the probabilities reported in Table 8 are comfortably small. In addition, many of the compact families show clustered orbital longitudes and past convergence (see below); this includes the family around (9332) 1990SB1 (Table 8). The statistical significance of these families would greatly increase if these properties were taken into account.

The three most problematic families are: (240) Vanadis (17 members, 0.003 probability), (22766) 1999AE7 (5 members, 0.01 probability) and (77882) 2001 SV124 (316 members, 0.05 probability). We prefer to report these families here but acknowledge that these cases need a more detailed analysis and/or confirmation from additional data. It is useful to include them here to see whether these borderline cases will or will not be confirmed with new data. The (77882) 2001 SV124 family is one of only two larger families (with more than 20 members) – the other one being (106) Dione – that are listed in Table 8.

We now comment on several new families of special interest. Notably, the family around (1461) Jean-Jacques in the outer belt is interesting because this object, 30-40 km in diameter, is classified as a metallic M-type asteroid in Tholen taxonomy. Another interesting case is a new family in the inner belt near asteroids (2110) Moore-Sitterly and (44612) 1999 RP27. This family has 17 members that show obvious clustering in the perihelion and nodal longitudes (Table 9). Pravec & Vokrouhlický (2009) (see also Pravec et al. 2010), identified the two largest bodies in the family, 2110 and 44612, as an asteroid pair (Vokrouhlický & Nesvorný 2008). Polishook et al. (2014a,b) found their spectral classification as intermediate between S and Sq. They have rotation periods 3.345 hr and 4.907 hr, respectively, and both are retrograde rotators with poles pointing to ecliptic latitudes between -70° and -80° (Pravec et al. 2010, 2019; Polishook 2014).

Figure 9 shows osculating orbits of the Moore-Sitterly family members. The two largest bodies, 2110 and 44612, have slightly larger semimajor axis values than the rest of the family. There is an obvious orbital convergence of secular angles 1.2-1.5 Myr ago (Fig. 10), which clearly demonstrates that this family must be very young. We find that the semimajor axis difference between 2110 and 44612 corresponds to the ejection velocity of ~ 2 m/s, which is comparable to the escape velocity from (2110) Moore-Sitterly. Some of the small fragments are ~ 10 times farther away, which would indicate an ejection velocity of ~ 20 m/s – much larger than the escape velocity – and this would be puzzling. If all small fragments were retrograde rotators, however, their displacement could be explained by the Yarkovsky drift sunward from their original locations over 1.2-1.5 Myr. The magnitude distribution of the family members (Table 9) indicates a notable separation between the two largest members (formerly found to constitute a pair of asteroids), and the smaller fragments. This is reminiscent of the Hobson family case (e.g., Vokrouhlický et al. 2021), where the authors speculated that the parent body of the Hobson family was a binary asteroid. Indeed, the nearly equal-size binaries should represent some 15% of $D < 10$ km main belt asteroids (e.g., Pravec et al. 2016), and it is inevitable that some of the binaries give birth to families.

These same analysis was applied all families listed as "compact" in Tables 3-7. We do not comment on these cases in detail here, this will be the subject of a separate publication, but point out that the new families (1217) Maximiliana, (6084) Bascom, (10164) Akusekijima and (70208) 1999RX33 show past convergence of orbital longitudes, and are estimated here

to have formed 0.5-2.5 Myr ago.

We also identify the youngest asteroid family found in the main belt so far. Asteroid (9332) 1990SB1 with $H = 13.2$ ($D = 6.8$ km for a reference albedo $p_V = 0.2$), $a = 2.583$ au, $e = 0.107$, $i = 12.65$ deg (osculating elements), is a member of the large Eunomia family in the middle main belt (Nesvorný et al. 2015). It has a relatively short rotation period, 2.987 hr, and the lightcurve amplitude of 0.39 mag. Pravec et al (2019) found it is a binary; the satellite has an orbital period of 48.84 hr. Now, there are 8 small asteroids near (9332) 1990SB1 with very similar orbits (Table 10 and Fig. 11). We integrated their orbits backward in time and established that the family formed only 16-17 kyr ago (Fig. 12). This is younger than the previous record holder, the (5026) Martes family (Vokrouhlický et al. 2024), with the estimated age of $\simeq 18.1$ kyr. Assuming that the (9332) 1990SB1 family and satellite around (9332) 1990SB1 formed at the same time, we now know the age of the binary as well. This may be useful to understanding the binary formation, and evolution of binary orbits by tides and non-gravitational effects. We will report a more thorough analysis of this case in forthcoming publications.

5. Conclusions

The main findings of this work are summarized as follows:

1. The proper elements of asteroids are computed from the Fourier method (Šidlichovský & Nesvorný 1996, Knežević & Milani 1999). We speed up and improve the computation by using the symplectic integrator/corrector and Frequency Modified Fourier Transform (Šidlichovský & Nesvorný 1996).
2. The new catalog of proper elements for 1.25×10^6 main belt asteroids is available at <https://asteroids.on.br/appeal/>, www.boulder.swri.edu/~davidn/Proper24/, and the Planetary Data System (PDS) node, <https://pds.nasa.gov/>.
3. A search for collisional families yielded 153 cases not reported in Nesvorný et al. (2015): 31 in the inner belt, 48 in the middle belt, 17 in the pristine zone, 39 in the outer belt, and 18 in high inclinations. 136 of these cases are new discoveries and 17 were identified

in various other publications. There are now 274 known families in the asteroid belt in total (the Hilda families are not included here).

4. The (2110) Moore-Sitterly family is a close pair of relatively large bodies, 2110 and 44612, and 15 small members all located sunwards from 2110 and 44612, presumably a consequence of the Yarkovsky drift over the estimated family age (1.2-1.5 Myr).
5. New families (1217) Maximiliana, (6084) Bascom, (10164) Akusekijima and (70208) 1999RX33 are estimated to have formed 0.5-2.5 Myr ago. The new family around outer belt asteroid (1461) Jean-Jacques is interesting because this object is classified as a metallic M-type in the Tholen taxonomy.
6. The new family around middle belt asteroid (9332) 1990SB1 has 9 members. It is the youngest family found in the asteroid belt so far (estimated formation only 16-17 kyr ago). Asteroid (9332) 1990SB1 itself is a binary (Pravec et al 2019).

A systematic characterization of new asteroid families is left for future work.

The methodology described here offers a practical method to compute asteroid proper elements for the large amount of data expected from the Rubin Observatory (Schwamb et al. 2023). There are two improvements. First, the symplectic integrator/corrector can speed up the computation of proper elements by a factor of ~ 5 .¹⁷ The exact speed-up factor depends on the timestep used in the N -body integrator. Here we use a conservatively short timestep (1.1 day) but point out that symplectic timesteps up to $\simeq 5$ days can yield accurate proper elements. Second, the massive parallelization on 10,000+ cores of the NASA Pleiades Supercomputer (as demonstrated here, implemented via a PBS script; also see Novaković et al. 2009) will allow us to compute the proper elements for 10^7 main-belt asteroids in under a month of wall-clock time.

¹⁷The beauty of symplectic integrators is that they can be used with time steps up to $\sim 1/20$ of the shortest orbital period and that without any excessive growth of the integration error. Here we used a conservatively short time step, about $1/80$ of the orbital period of Mercury, and verified that that the method works well – with only a modest effect on the accuracy of proper elements – for time steps as long as 5 days. Compared to that, the multistep predictor in the ORBIT9 integrator uses a time step that is typically $\sim 1/100$ of the shortest orbital period (Milani & Nobili 1988); this would correspond to ~ 21 hours for the orbital integration with Mercury. Therefore, since the ORBIT9 integrator needs to evaluate the gravitational accelerations up to ~ 5 times more often than the `Swift` integrator, the speed up can be as large as the factor of ~ 5 .

6. Appendix A: Frequency splitting

Here we illustrate the frequency splitting in the case of asteroid (5) Astraea. This issue has been reported in Šidlichovský & Nesvorný (1996) who found that (5) Astraea has a chaotic orbit near the secular resonance $g + g_5 - 2g_6 \simeq 0$, where g , g_5 and g_6 are the perihelion precession frequencies of asteroid, Jupiter and Saturn, respectively. Due to the resonance, the orbital eccentricity of (5) Astraea has large oscillations and a long term trend (Fig. A1). The resonant angle, $\sigma = \varpi + \varpi_5 - 2\varpi_6$, can undergo transitions between libration and circulation on long timescales (Šidlichovský & Nesvorný 1996); it is therefore not possible to obtain a unique decomposition of $e(t)$ into a quasi-periodic signal. Indeed, if we defined the proper eccentricity as the amplitude of the (largest) proper term, the proper eccentricity value would depend on the Fourier window that is used in FMFT. For example, for a 0.6-Myr window the amplitude of the proper term is $\simeq 0.24$ (Fig. A2). For a 5-Myr window, the proper term undergoes splitting into several terms with similar amplitudes; the amplitude of the largest term is $\simeq 0.12$. The length of the Fourier window defines how many terms appear and affects the amplitude of the largest term as well. It is difficult, using this method, to define a unique value of e_p . For reference, the method described in Section 2.1 gives $e_p = 0.171 \pm 0.012$ for (5) Astraea.

Acknowledgments

The simulations were performed on the NASA Pleiades Supercomputer. We thank the NASA NAS computing division for continued support. The work of DN was funded by the NASA SSW program. DV acknowledges support from the grant 23-04946S of the Czech Science Foundation. FR acknowledges support from CNPq grant 312429/2023-1. We thank an anonymous reviewer for critical comments.

REFERENCES

- Brož, M. & Vokrouhlický, D. 2008, MNRAS, 390, 715. doi:10.1111/j.1365-2966.2008.13764.x
- Brož, M., Vokrouhlický, D., Morbidelli, A., et al. 2011, MNRAS, 414, 2716. doi:10.1111/j.1365-2966.2011.18587.x

- Brož, M., Vernazza, P., Marsset, M., et al. 2024, arXiv:2403.08552.
doi:10.48550/arXiv.2403.08552
- Carruba, V., Nesvorný, D., Aljbaae, S., et al. 2015, MNRAS, 451, 244.
doi:10.1093/mnras/stv997
- Carruba, V., Nesvorný, D., & Aljbaae, S. 2016, Icarus, 271, 57.
doi:10.1016/j.icarus.2016.01.006
- Carruba, V., Aljbaae, S., & Lucchini, A. 2019, MNRAS, 488, 1377.
doi:10.1093/mnras/stz1795
- Dykhuys, M. J. & Greenberg, R. 2015, Icarus, 252, 199. doi:10.1016/j.icarus.2015.01.012
- Farley, K. A., Vokrouhlický, D., Bottke, W. F., et al. 2006, Nature, 439, 295.
doi:10.1038/nature04391
- Knežević, Z. & Milani, A. 2000, Celestial Mechanics and Dynamical Astronomy, 78, 17.
doi:10.1023/A:1011187405509
- Knežević, Z. & Milani, A. 2019, Celestial Mechanics and Dynamical Astronomy, 131, 27.
doi:10.1007/s10569-019-9906-4
- Laskar, J. 1993, Celestial Mechanics and Dynamical Astronomy, 56, 191.
doi:10.1007/BF00699731
- Levison, H. F. & Duncan, M. J. 1994, Icarus, 108, 18. doi:10.1006/icar.1994.1039
- Milani, A. & Nobili, A. M. 1988, Celestial Mechanics, 43, 1. doi:10.1007/BF01234550
- Milani, A. & Knezevic, Z. 1994, Icarus, 107, 219. doi:10.1006/icar.1994.1020
- Milani, A., Cellino, A., Knežević, Z., et al. 2014, Icarus, 239, 46.
doi:10.1016/j.icarus.2014.05.039
- Nesvorný, D., Bottke, W. F., Dones, L., et al. 2002, Nature, 417, 720.
doi:10.1038/nature00789

- Nesvorný, D., Brož, M., & Carruba, V. 2015, *Asteroids IV*, 297. doi:10.2458/azu-uapress_9780816532131-ch016
- Novaković, B. & Radović, V. 2019, *Research Notes of the American Astronomical Society*, 3, 105. doi:10.3847/2515-5172/ab3460
- Novaković, B., Balaz, A., Knežević, Z., et al. 2009, *Serbian Astronomical Journal*, 179, 75. doi:10.2298/SAJ0979075N
- Novaković, B., Cellino, A., & Knežević, Z. 2011, *Icarus*, 216, 69. doi:10.1016/j.icarus.2011.08.016
- Novaković, B., Hsieh, H. H., Cellino, A., et al. 2014, *Icarus*, 231, 300. doi:10.1016/j.icarus.2013.12.019
- Novaković, B., Vokrouhlický, D., Spoto, F., et al. 2022, *Celestial Mechanics and Dynamical Astronomy*, 134, 34. doi:10.1007/s10569-022-10091-7
- Nugent, C. R., Mainzer, A., Masiero, J., et al. 2015, *ApJ*, 814, 117. doi:10.1088/0004-637X/814/2/117
- Park, R. S., Folkner, W. M., Williams, J. G., et al. 2021, *AJ*, 161, 105. doi:10.3847/1538-3881/abd414
- Parker, A., Ivezić, Ž., Jurić, M., et al. 2008, *Icarus*, 198, 138. doi:10.1016/j.icarus.2008.07.002
- Polishook, D. 2014, *Icarus*, 241, 79. doi:10.1016/j.icarus.2014.06.018
- Polishook, D., Moskovitz, N., Binzel, R. P., et al. 2014a, *Icarus*, 233, 9. doi:10.1016/j.icarus.2014.01.014
- Polishook, D., Moskovitz, N., DeMeo, F. E., et al. 2014b, *Icarus*, 243, 222. doi:10.1016/j.icarus.2014.08.010
- Pravec, P. & Vokrouhlický, D. 2009, *Icarus*, 204, 580. doi:10.1016/j.icarus.2009.07.004
- Pravec, P., Vokrouhlický, D., Polishook, D., et al. 2010, *Nature*, 466, 1085. doi:10.1038/nature09315

- Pravec, P., Scheirich, P., Kušnirák, P., et al. 2016, *Icarus*, 267, 267. doi:10.1016/j.icarus.2015.12.019
- Pravec, P., Fatka, P., Vokrouhlický, D., et al. 2019, *Icarus*, 333, 429. doi:10.1016/j.icarus.2019.05.014
- Quinn, T. R., Tremaine, S., & Duncan, M. 1991, *AJ*, 101, 2287. doi:10.1086/115850
- Rozehnal, J., Brož, M., Nesvorný, D., et al. 2016, *MNRAS*, 462, 2319. doi:10.1093/mnras/stw1719
- Schwamb, M. E., Jones, R. L., Yoachim, P., et al. 2023, *ApJS*, 266, 22. doi:10.3847/1538-4365/acc173
- Šidlichovský, M. & Nesvorný, D. 1996, *Celestial Mechanics and Dynamical Astronomy*, 65, 137. doi:10.1007/BF00048443
- Tsiganis, K., Knežević, Z., & Varvoglis, H. 2007, *Icarus*, 186, 484. doi:10.1016/j.icarus.2006.09.017
- Tsirvoulis, G. 2019, *MNRAS*, 482, 2612. doi:10.1093/mnras/sty2898
- Tsirvoulis, G. & Novaković, B. 2016, *Icarus*, 280, 300. doi:10.1016/j.icarus.2016.06.024
- Vokrouhlický, D. & Nesvorný, D. 2008, *AJ*, 136, 280. doi:10.1088/0004-6256/136/1/280
- Vokrouhlický, D., Durech, J., Michałowski, T., et al. 2009, *A&A*, 507, 495. doi:10.1051/0004-6361/200912696
- Vokrouhlický, D., Brož, M., Novaković, B., et al. 2021, *A&A*, 654, A75. doi:10.1051/0004-6361/202141691
- Vokrouhlický, D., Nesvorný, D., Brož, M., et al. 2024, *A&A*, 681, A23. doi:10.1051/0004-6361/202347670
- Wisdom, J. 2006, *AJ*, 131, 2294. doi:10.1086/500829
- Wisdom, J. & Holman, M. 1991, *AJ*, 102, 1528. doi:10.1086/115978

Zappalà, V., Cellino, A., Farinella, P., et al. 1990, *AJ*, 100, 2030. doi:10.1086/115658

Zappala, V., Cellino, A., Farinella, P., et al. 1994, *AJ*, 107, 772. doi:10.1086/116897

j	g_j	s_j
	arcsec/s	arcsec/s
1	5.535	-5.624
2	7.437	-7.082
3	17.357	-18.837
4	17.905	-17.749
5	4.257	–
6	28.245	-26.348
7	3.088	-2.993
8	0.671	-0.692

Table 1: The secular precession frequencies of the planetary system determined from a 10-Myr-long numerical integration.

a_p au	δa_p au	e_p	δe_p	$\sin i_p$	$\delta \sin i_p$	g arcsec/s	s arcsec/s	H mag	# of opps.	MPC desig.
2.767028	0.23E-04	0.115193	0.16E-03	0.167560	0.13E-04	54.253800	-59.249995	3.340	123	00001
2.771276	0.12E-03	0.280234	0.34E-03	0.546016	0.45E-04	-1.372312	-46.451120	4.120	121	00002
2.669376	0.75E-05	0.233600	0.95E-05	0.229144	0.25E-05	43.858531	-61.476025	5.170	114	00003
2.361512	0.59E-07	0.099452	0.14E-03	0.111023	0.18E-03	36.882605	-39.610314	3.220	110	00004
2.577657	0.29E-04	0.171249	0.12E-01	0.076113	0.14E-02	52.506470	-51.132322	7.000	87	00005
2.425275	0.15E-05	0.158950	0.13E-03	0.249017	0.52E-03	31.540156	-41.819571	5.610	103	00006
2.386116	0.27E-04	0.210605	0.51E-03	0.108920	0.48E-03	38.458755	-46.352563	5.640	90	00007
2.201393	0.20E-04	0.144783	0.12E-03	0.096433	0.17E-03	32.049097	-35.508300	6.610	94	00008
2.386436	0.32E-05	0.127508	0.84E-04	0.081626	0.49E-04	38.763873	-42.014077	6.320	86	00009
3.141917	0.59E-04	0.135147	0.93E-04	0.088733	0.49E-05	128.714227	-97.051050	5.640	99	00010
2.452256	0.18E-06	0.074519	0.22E-04	0.067789	0.15E-04	40.764583	-43.166575	6.730	105	00011
2.334262	0.39E-04	0.174974	0.64E-04	0.162217	0.61E-04	34.152919	-40.893417	7.310	82	00012
2.576296	0.12E-05	0.126367	0.11E-03	0.276336	0.48E-04	35.937744	-45.446496	6.930	74	00013
2.587547	0.14E-05	0.198285	0.15E-04	0.145452	0.59E-04	48.841992	-56.278925	6.560	84	00014
2.643475	0.32E-05	0.148582	0.81E-04	0.226506	0.50E-04	42.699508	-52.035733	5.410	84	00015
2.922133	0.76E-05	0.102836	0.23E-03	0.044006	0.24E-04	76.932586	-73.291465	6.210	93	00016
2.471116	0.71E-05	0.137893	0.16E-04	0.084985	0.30E-04	43.752221	-46.311410	7.940	96	00017
2.295882	0.14E-03	0.178486	0.57E-04	0.169080	0.46E-04	32.651574	-39.374445	6.340	85	00018
2.442013	0.17E-06	0.134582	0.17E-04	0.038793	0.24E-04	41.875606	-45.185309	7.500	96	00019
2.408640	0.80E-05	0.161834	0.28E-04	0.024686	0.46E-04	40.879490	-45.112965	6.540	92	00020

Table 2: The full proper element catalog is available for download at <https://asteroids.on.br/appeal/> and www.boulder.swri.edu/~davidn/Proper24/.

Number	Name	HCM cut (m/s)	number of mem.	Notes
6	Hebe	80	112	compact, depleted, S-type
40	Harmonia	70	160	extended, 40 is offset, S-type
67	Asia	40	569	diffuse, S-type
115	Thyra	30	56	compact, S-type
126	Velleda	70	308	extended, close to 1394, S-type
135	Hertha	20	1473	in Nysa, big, Dykhuis et al. (2015)
345	Tercidina	80	429	diffuse, extended in <i>a</i> , S-type
1156	Kira	70	33	small, S-type
1217	Maximiliana	20	28	small, convergent
1394	Algoa	50	27	small, close to 126, S-type
1598	Paloque	40	117	compact, big bodies, C-type
1663	van der Bos	30	285	in Flora, diffuse
1963	Bezovec	65	354	in Phocaea, diffuse, offset
2110	Moore-Sitterly	10	17	compact, convergent, S-type
2328	Robeson	20	223	compact, C-type
2653	Principia	50	131	near Vesta, compact, S-type
2728	Yatskiv	30	48	in Polana, compact, C-type
2823	van der Laan	60	136	near Sulamitis, offset, S-type
2961	Katsurahama	25	142	in Flora, small
3452	Hawke	100	116	diffuse, depleted, 317?, C-type
6065	Chesneau	60	351	in Phocaea, diffuse, 587?
6084	Bascom	10	10	in Phocaea, very small, convergent
6142	Tantawi	30	114	in Polana, compact, Novaković & Radović (2019)
8272	Iitatemura	40	41	compact, S-type
18429	1994 AO1	20	38	compact, Novaković & Radović (2019)
41331	1999 XB232	20	23	in Phocaea, very small
61203	Chleborad	20	20	in Vesta, close to 3:1, compact
70208	1999 RX33	20	16	in Phocaea, very small, convergent
118564	2000 FO47	20	84	in Nysa, compact, S-type
484743	2008 YL101	30	16	compact
–	2012 PM61	15	35	in Vesta, compact, only small bodies

Table 3: 31 asteroid families – not listed in Nesvorný et al. (2015) – in the inner belt ($a < 2.5$ au). Three of these families (Hertha, Tantawi and 1994 AO1) were already reported in recent publications (Dykhuis et al. 2015, Novaković & Radović 2019). The HCM cutoff and number of family members identified at this cutoff are listed in columns 3 and 4, respectively. The HCM cutoffs reported here are approximate and will be fine tuned in future publications.

Number	Name	HCM cut (m/s)	number of mem.	Notes
28	Bellona	30	958	numerous small bodies
45	Eugenia	35	246	2 satellites, small bodies, diffuse, C-type
177	Irma	60	413	diffuse, K-type?
194	Prokne	50	176	194 is offset, Novaković et al. (2011)
237	Coelestina	40	104	small, S-type
240	Vanadis	60	17	near Misa, small, C-type, needs confirmation
342	Endymion	20	33	very small, close to Konig, C-type
351	Irsa	20	242	small bodies, S-type
389	Industria	50	464	big, S-type, offset
446	Aeternitas	40	447	big, compact
539	Pamina	37	81	diffuse, 539 is offset, C-type
593	Titania	40	297	small, C-type
660	Crescentia	20	805	in Maria, big
727	Nipponia	20	510	near Maria, compact, C-type
801	Helwerthia	40	175	big bodies, compact, C-type
1048	Fedosia	40	125	compact, C-type
1127	Mimi	60	82	small, 1127 is offset, C-type
1160	Illyria	30	692	in Maria, diffuse
1347	Patria	50	132	compact, 1347 is offset, C-type
2079	Jacchia	35	125	in Eunomia, diffuse
2927	Alamosa	20	14	very small
3324	Avsyuk	30	222	offset, S-type
3497	Innanen	50	261	small, C-type
3567	Alvema	55	260	extended, big bodies, C-type
5798	Burnett	58	81	extended, diffuse, S-type
7233	Majella	10	17	very small
7403	Choustnik	30	57	small, 7403 is offset, C-type
8223	Bradshaw	20	48	very small, C-type
9332	1990 SB1	10	8	in Eunomia, compact, convergent
10164	Akusekijima	10	18	compact, convergent
11014	Svatopluk	50	159	extended, small bodies, C-type
12586	Shukla	20	25	very small, S-type
15104	2000 BV3	30	78	small, C-type
16472	1990 OE5	7	58	in Dora, compact, C-type
16940	1998 GC3	20	40	in Eunomia, diffuse
21591	1998 TA6	15	47	in Eunomia, compact
22766	1999 AE7	10	5	compact, needs confirmation
26170	Kazuhiko	10	9	compact, S-type
30718	Records	40	95	diagonal, C-type
32983	1996 WU2	20	50	in Eunomia, small
42357	2002 CS52	40	216	compact, S-type
49362	1998 WW16	30	68	49362 is offset, S-type
53209	1999 CQ75	20	189	small, C-type
54934	2001 OH105	50	37	small bodies
190237	2007 DM10	50	41	small
249576	1995 FH2	30	78	diffuse, C-type
435544	2008 OV23	20	90	in Eunomia, compact, small bodies
–	2006 QX49	20	11	compact

Table 4: 48 asteroid families – not listed in Nesvorný et al. (2015) – in the middle belt ($2.5 < a < 2.82$ au). The Prokne family has already been reported in Novaković et al. (2011). The HCM cutoff and number of family members identified at this cutoff are listed in columns 3 and 4, respectively. The HCM cutoffs reported here are approximate and will be fine tuned in future publications.

Number	Name	HCM cut (m/s)	number of mem.	Notes
174	Phaedra	60	170	diffuse, S-type
321	Florentina	10	209	Koronis ₄ in Brož et al. (2024), HCM cut
392	Wilhelmina	40	45	compact, C-type
924	Toni	50	50	compact, C-type
1289	Kutaisii	10	371	Koronis ₃ in Brož et al. (2024)
3787	Aivazovskij	15	12	in Itha, compact
4471	Graculus	50	136	small, S-type
11048	1990 QZ5	50	35	extended in e , compact in i
15454	1998 YB3	50	340	large bodies, C-type
19093	1979 MM3	90	71	split of 709 Fringilla (FIN 623)
26369	1999 CG62	50	43	small, C-type
31810	1999 NR38	60	103	diffuse, S-type
37981	1998 HD130	90	419	split of 709 Fringilla (FIN 623)
77873	2001 SQ46	50	21	small, C-type
78225	2002 OS10	60	88	diffuse
211772	2004 BQ90	70	295	diffuse, C-type
217472	2005 WV105	40	37	small

Table 5: 17 asteroid families – not listed in Nesvorný et al. (2015) – in the pristine zone ($2.82 < a < 2.96$ au). The Florentina and Kutaisii families were reported in Brož et al. (2024) as Koronis₄ and Koronis₃, respectively. The (19093) 1979MM3 and (37981) 1998HD130 families are a split of the (709) Fringilla family (FIN 623; Nesvorný et al. 2015) into two parts. The HCM cutoff and number of family members identified at this cutoff are listed in columns 3 and 4, respectively. The HCM cutoffs reported here are approximate and will be fine tuned in future publications.

Number	Name	HCM cut (m/s)	number of mem.	Notes
52	Europa	50	250	diffuse, C-type
106	Dione	55	261	extended, diffuse, 3136?
260	Huberta	70	190	extended, C-type, Cybeles, Carruba et al. (2015)
286	Iclea	50	143	compact, C-type
414	Liriope	70	14	compact, depleted, Cybeles
633	Zelima	10	88	in Eos, compact, z_1 resonance, Tsirvoulis (2019)
690	Wratislavia	30	820	big, C-type
850	Altona	60	73	depleted
885	Ulrike	30	45	compact, C-type
991	McDonalda	20	260	in Themis, diffuse
1323	Tugela	50	412	big, C-type, 1323 offset, 69559 in Novaković et al. (2011)
1357	Khama	30	62	compact, C-type
1461	Jean-Jacques	30	174	compact, numerous small bodies, M-type?
1524	Joensuu	40	201	K-type?
1599	Giomus	25	322	in Hygiea
2458	Veniakaverin	30	177	in Themis
2562	Chaliapin	22	271	in Eos, diffuse
3310	Patsy	15	826	in Eos, compact
3803	Tuchkova	10	7	small, C-type
4291	Kodaihasu	20	16	compact
4897	Tomhamilton	20	254	in Eos, 4897 is offset, diffuse
5228	Maca	30	47	in Themis, very small
6924	Fukui	80	146	extended, C-type, Cybeles, Carruba et al. (2019)
7504	Kawakita	10	19	small, C-type
8737	Takehiro	40	569	8737 is offset, HCM cut
9522	Schlichting	100	9	only a few big bodies, Cybeles, Carruba et al. (2019)
12911	Goodhue	18	132	in Themis
20674	1999 VT1	10	35	compact, 20674 offset, Gibbs in Novaković et al. (2014)
29880	Andytran	20	44	in Themis
34216	2000 QK75	20	22	small, C-type
37455	4727 P-L	40	285	37455 is offset, C-type
48412	1986 QN1	60	100	compact
48506	1993 FO10	20	90	near Tirela, C-type
63235	2001 BV20	60	35	small, C-type, Cybeles
77882	2001 SV124	45	316	diffuse, HCM cuts, needs confirmation
106302	2000 UJ87	30	489	extended, C-type, 86 is offset, 13:6 diffusion?
157940	1999 XU240	10	19	compact, low number of bodies
352479	2008 BO31	30	50	small
365736	2010 WK8	50	40	small, C-type, Cybeles

Table 6: 39 asteroid families – not listed in Nesvorný et al. (2015) – in the outer belt ($a > 2.96$ au). Five of these families (Huberta, Zelima, Tugela, Fukui, Schlichting, Gibbs/1999 VT1) were already reported in previous publications (Novaković et al. 2011, 2014; Carruba et al. 2015, 2019; Tsirvoulis 2019). The HCM cutoff and number of family members identified at this cutoff are listed in columns 3 and 4, respectively. The HCM cutoffs reported here are approximate and will be fine tuned in future publications.

Number	Name	HCM cut (m/s)	number of mem.	Notes
183	Istria	80	301	big, S-type
350	Ornamenta	70	716	in Alauda, big, extended, C-type, 130?
386	Siegena	100	168	extended, C-type
522	Helga	200	34	extended, C-type, Cybeles, Carruba et al. (2015)
704	Interamnia	50	413	offset, cratering?, C-type
754	Malabar	60	79	extended, also big bodies, C-type
1312	Vassar	30	21	C-type, Novaković et al. (2011)
1390	Abastumani	40	65	small, C-type, Cybeles, Carruba et al. (2019)
3001	Michelangelo	200	42	dispersed, no background
3854	George	130	261	in Hungarias, extended, diffuse, S-type
7605	Cindygraber	30	85	small, C-type, Novaković et al. (2011)
63530	2001 PG20	90	419	extended, C-type
77899	2001 TS117	200	257	very extended, low-density, 77899 is offset, M-type?
78705	2002 TE180	10	24	compact, S-type
101567	1999 AW22	50	293	extended, C-type? 116763 in Novaković et al. (2011)
126948	2002 FX3	30	14	compact, low number of bodies, C-type
236657	2006 KU114	70	303	extended, C-type
316974	2001 FP147	150	53	dispersed, no background, C-type

Table 7: 18 asteroid families – not listed in Nesvorný et al. (2015) – with high orbital inclinations ($\sin i > 0.3$). Five of these families (Helga, Vassar, Abastumani, Cindygraber, 116763/1999 AW22) were already reported in previous publications (Novaković et al. 2011, Carruba et al. 2019). The HCM cutoff and number of family members identified at this cutoff are listed in columns 3 and 4, respectively. The HCM cutoffs reported here are approximate and will be fine tuned in future publications.

Number	Name	Probability
106	Dione	1×10^{-6}
240	Vanadis	0.003
414	Liriope	2×10^{-6}
2110	Moore-Sitterly	2×10^{-7}
2927	Alamosa	3×10^{-7}
3787	Aivazovskij	6×10^{-6}
3803	Tuchkova	6×10^{-4}
6084	Bascom	5×10^{-5}
7233	Majella	2×10^{-7}
9332	1990SB1	0.02
9522	Schlichting	5×10^{-5}
22766	1999AE7	0.01
26170	Kazuhiko	3×10^{-4}
77882	2001SV124	0.05
126948	2002FX3	3×10^{-7}
–	2006 QX49	7×10^{-6}

Table 8: Asteroid families for which we were able to distinguish the statistical significance from 1 (from 10^7 trials with the box method; see Sect. 2.2). The third column reports the probability that random fluctuations of bodies in the local background could produce the family in question.

MPC desig.	H (mag)	a (au)	e	i (deg)	Ω (deg)	ω (deg)	M (deg)
02110	13.63	2.1980514	0.1770290	1.13155	140.45313	192.69746	338.26094
44612	15.67	2.1976575	0.1779052	1.12194	141.53740	189.48402	207.21536
X8073	18.66	2.1965096	0.1762623	0.88896	159.45456	160.96067	230.71251
q9915	18.75	2.1974504	0.1763956	0.91317	157.56482	163.77923	87.46958
K01K82Y	19.10	2.1969377	0.1759087	0.93567	155.79653	166.29243	347.34205
K02F44D	18.79	2.1965174	0.1770381	0.92887	155.96118	166.21130	135.31503
K06UN8L	19.35	2.1958976	0.1755210	0.83123	165.46635	151.66292	182.21323
K10RG7V	19.54	2.1970673	0.1740991	0.78330	170.10353	145.11975	82.11909
K13V79C	19.13	2.1961976	0.1770934	0.93426	156.16395	165.77682	133.44064
K14Qw7S	19.75	2.1959868	0.1753686	0.88033	161.03410	158.30843	356.31624
K15RJ4A	19.17	2.1964264	0.1750963	0.82816	165.61774	151.71076	258.86629
K15T83O	19.20	2.1968660	0.1762778	0.92017	156.87362	164.62329	273.37375
K16S14Q	19.29	2.1961233	0.1768452	0.91131	157.83567	163.15490	140.52663
K19O06U	19.90	2.1955252	0.1751064	0.79545	168.73592	147.83085	158.42254
K19SB1L	19.48	2.1956555	0.1752386	0.79853	168.11064	147.76117	185.50486
K21N62V	19.93	2.1961285	0.1740565	0.78380	170.20425	144.75362	292.68934
K22O48Q	19.43	2.1956928	0.1752722	0.81904	166.57575	149.94720	196.72505

Table 9: The osculating orbits of 17 members of the Moore-Sitterly family (MJD epoch 60400.0). Note the clustering of nodal (Ω) and perihelion (ω) longitudes.

MPC desig.	H (mag)	a (au)	e	i (deg)	Ω (deg)	ω (deg)	M (deg)
09332	13.24	2.5826279	0.1071552	12.64528	346.35641	211.88757	200.68128
~0EdI	18.11	2.5791555	0.1091825	12.69705	346.37901	210.86424	322.66213
K08CA6R	17.76	2.5795956	0.1090338	12.67301	346.36232	211.83755	277.44882
K10D44Y	17.74	2.5808240	0.1057713	12.65371	346.31579	211.24047	120.44629
K15Ra4C	18.02	2.5811666	0.1068327	12.64488	346.29494	211.84784	167.30554
K16D45B	17.99	2.5789990	0.1093170	12.69066	346.38013	211.21348	307.40249
K16E06Q	18.67	2.5790002	0.1093096	12.69115	346.38105	211.19633	308.01388
K17E36K	18.16	2.5826844	0.1076307	12.64840	346.34149	212.00629	234.08503
K17FJ3L	17.79	2.5817726	0.1080386	12.65332	346.33790	212.05776	245.77392

Table 10: The osculating orbits of 9 members of the (9332) 1990SB1 family (MJD epoch 60400.0). Note the clustering of nodal (Ω) and perihelion (ω) longitudes.

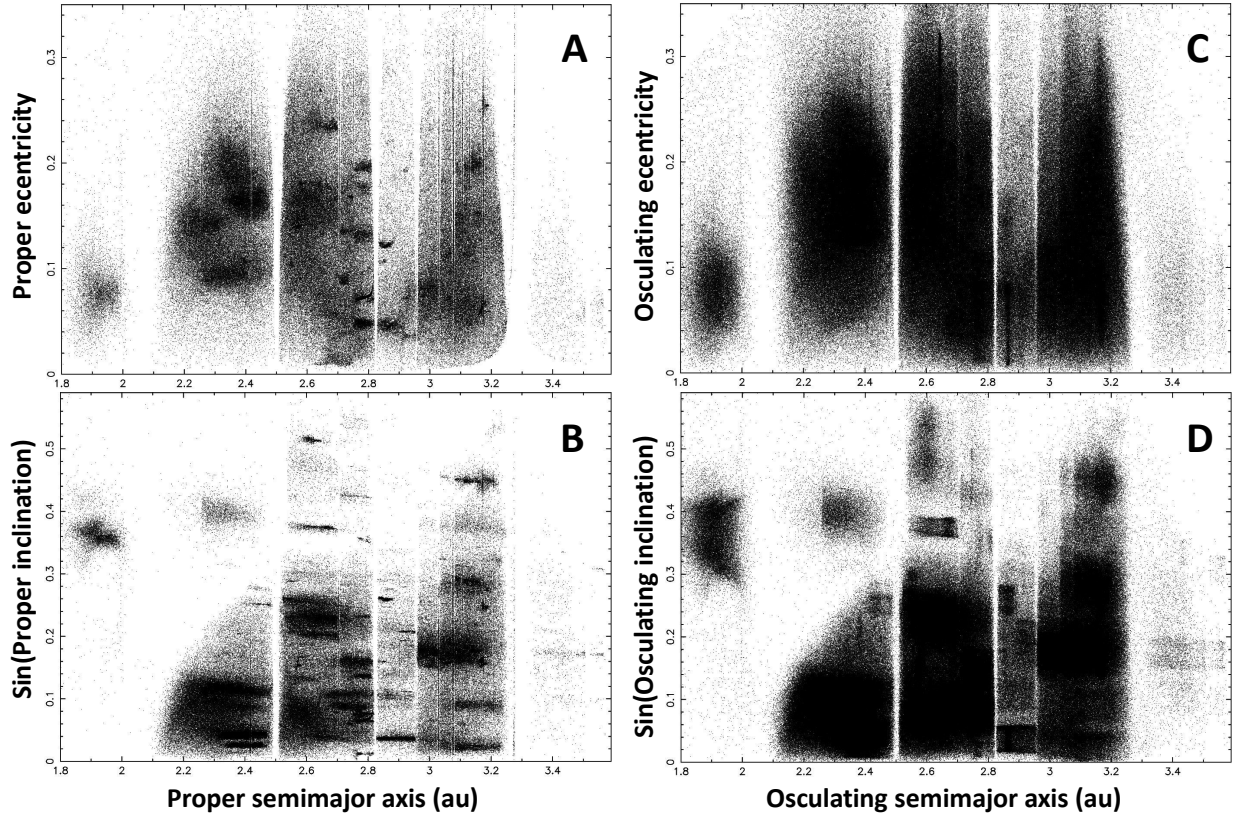


Fig. 1.— Proper (panels A and B) and osculating orbits (panels C and D) of main belt asteroids. In the proper element space, various orbital structures come into focus.

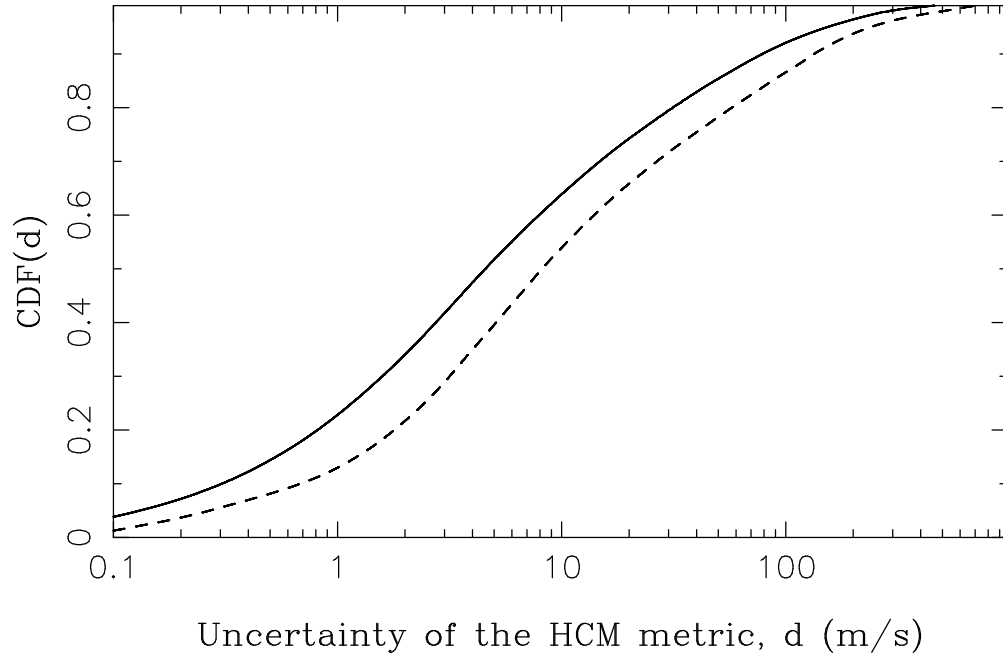


Fig. 2.— Uncertainties of proper elements in terms of the d metric: the new catalog (solid line), Novaković's AFP catalog (dashed line).

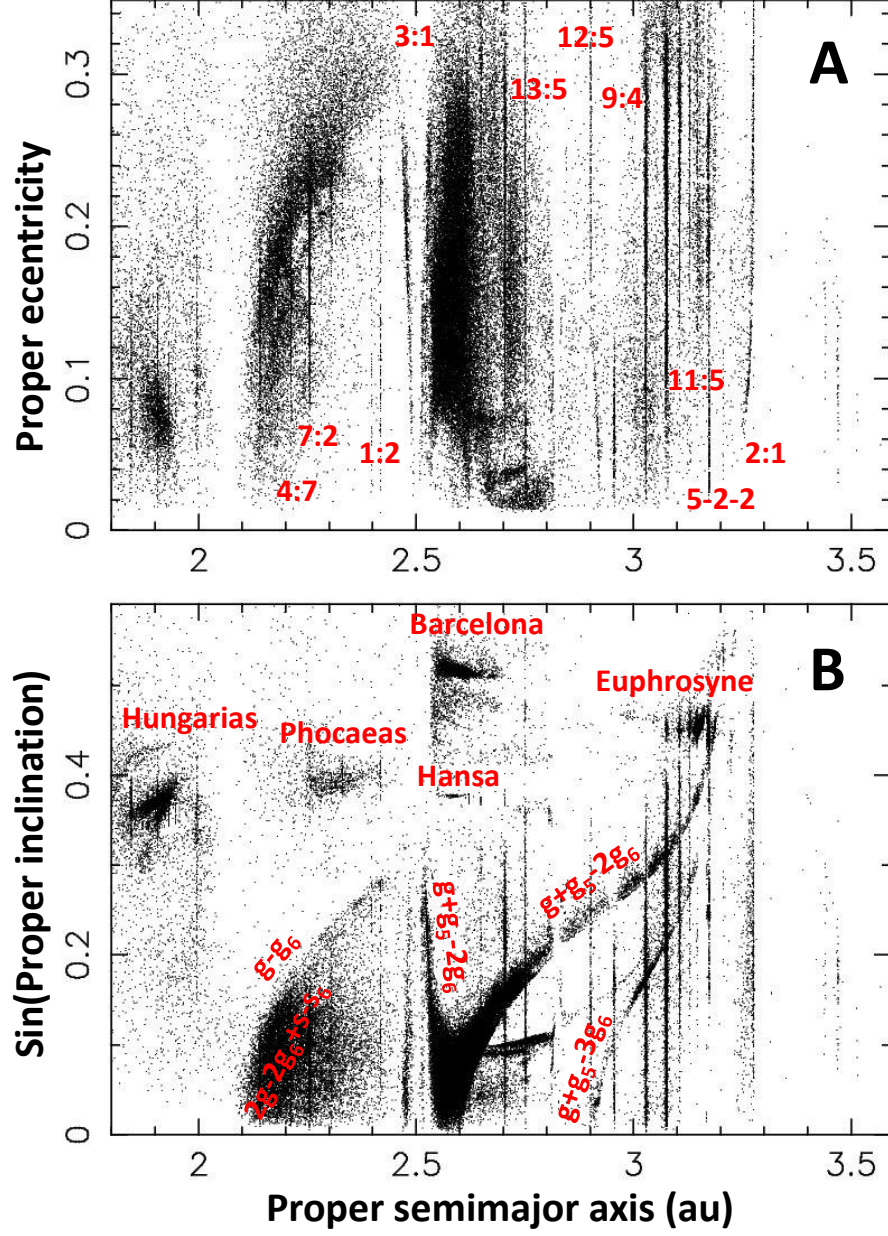


Fig. 3.— The proper orbits of main belt asteroids with relatively large errors ($d > 100$ m/s). Problematic mean motion resonances with Jupiter and Mars, secular resonances, and asteroid groups/families are labeled.

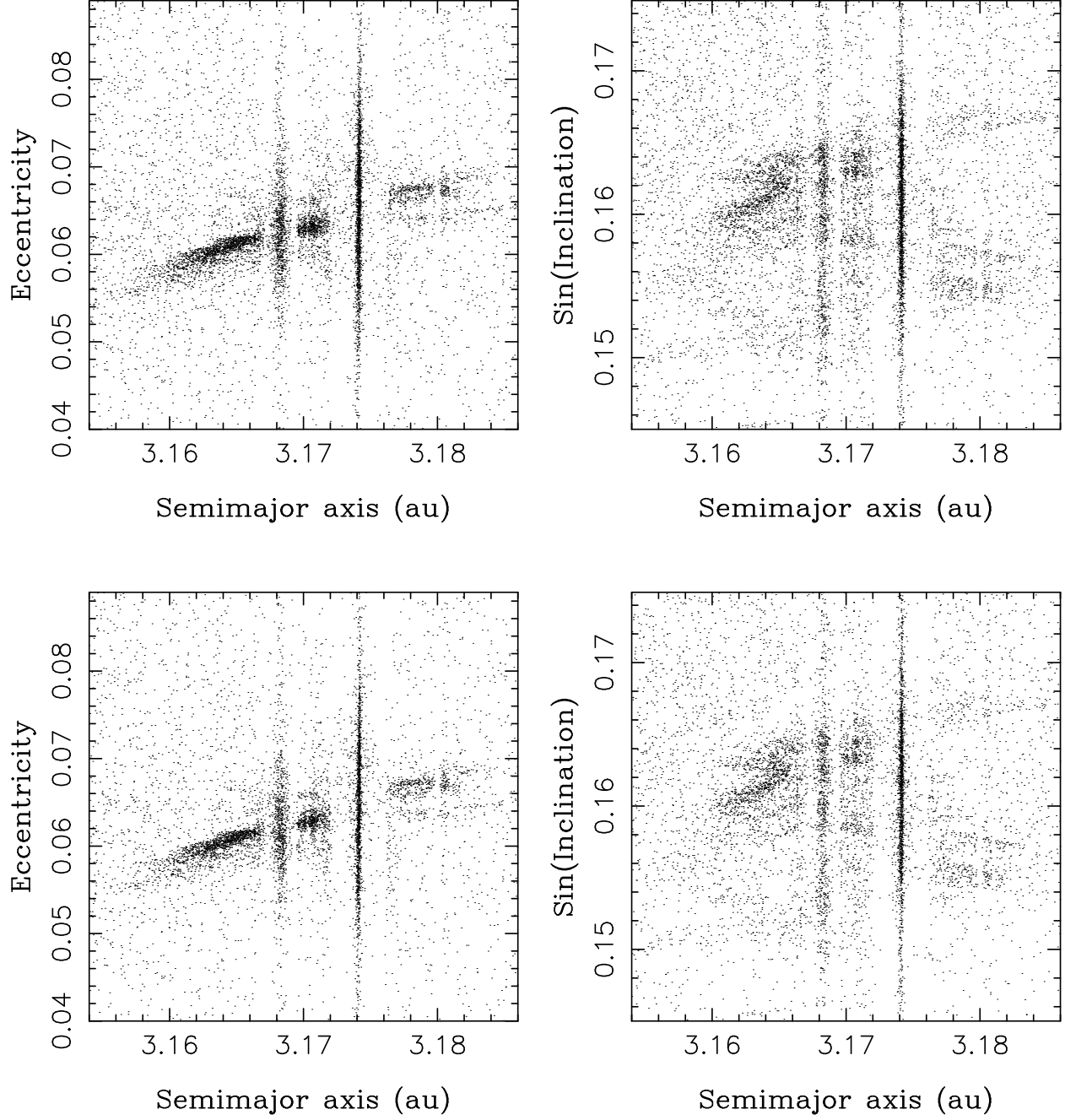


Fig. 4.— The dynamical structure of the Veritas family: the proper elements computed here (top panels) and the proper elements from <http://asteroids.matf.bg.ac.rs/fam/> (bottom panels).

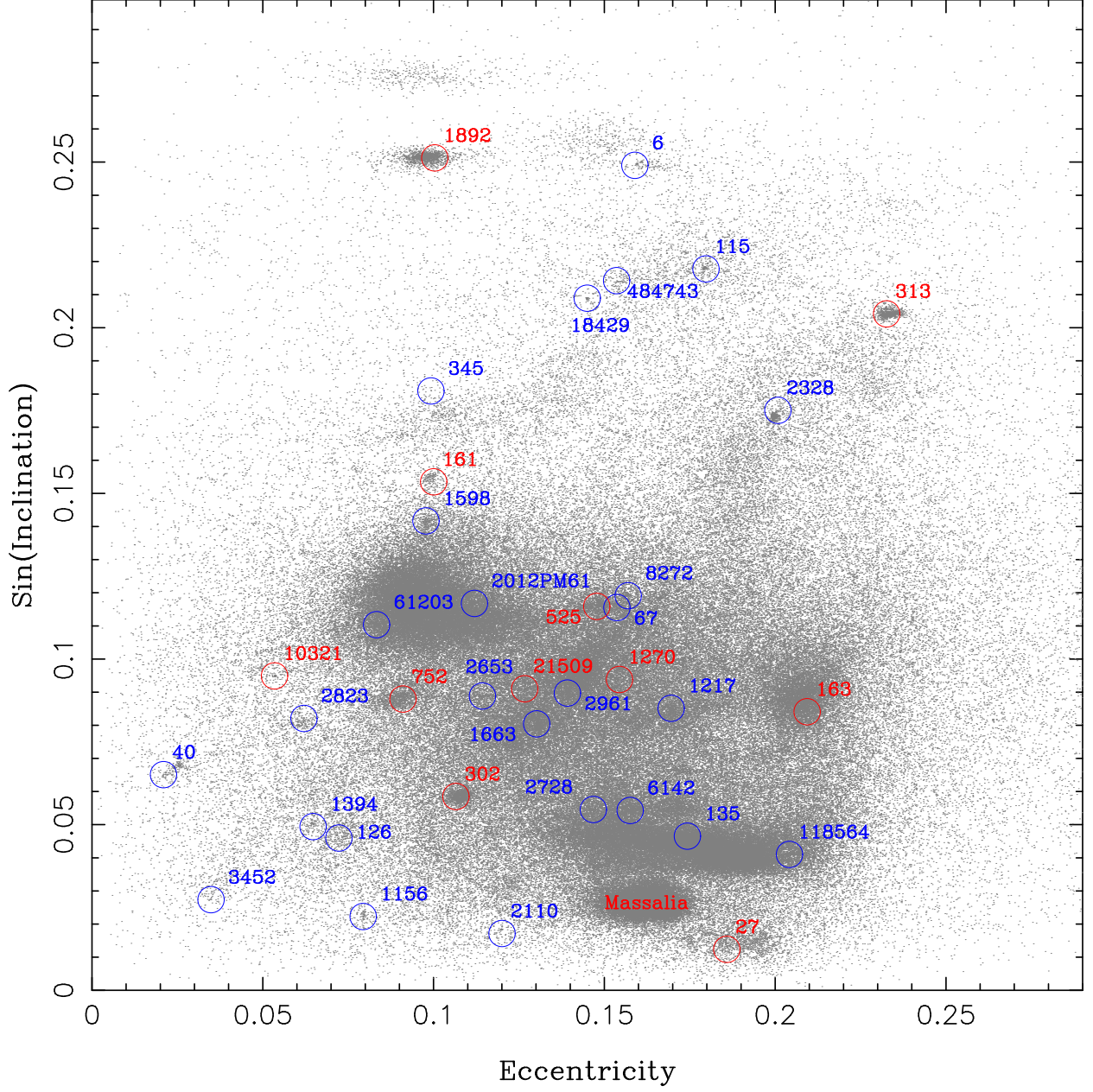


Fig. 5.— Proper eccentricities and sine of proper inclinations for inner belt asteroids ($a_p < 2.5$ au). Notable families are labeled: blue labels stand for families identified in this work and not listed in Nesvorný et al. (2015), red labels are families known previously (not all previously known families are labeled).

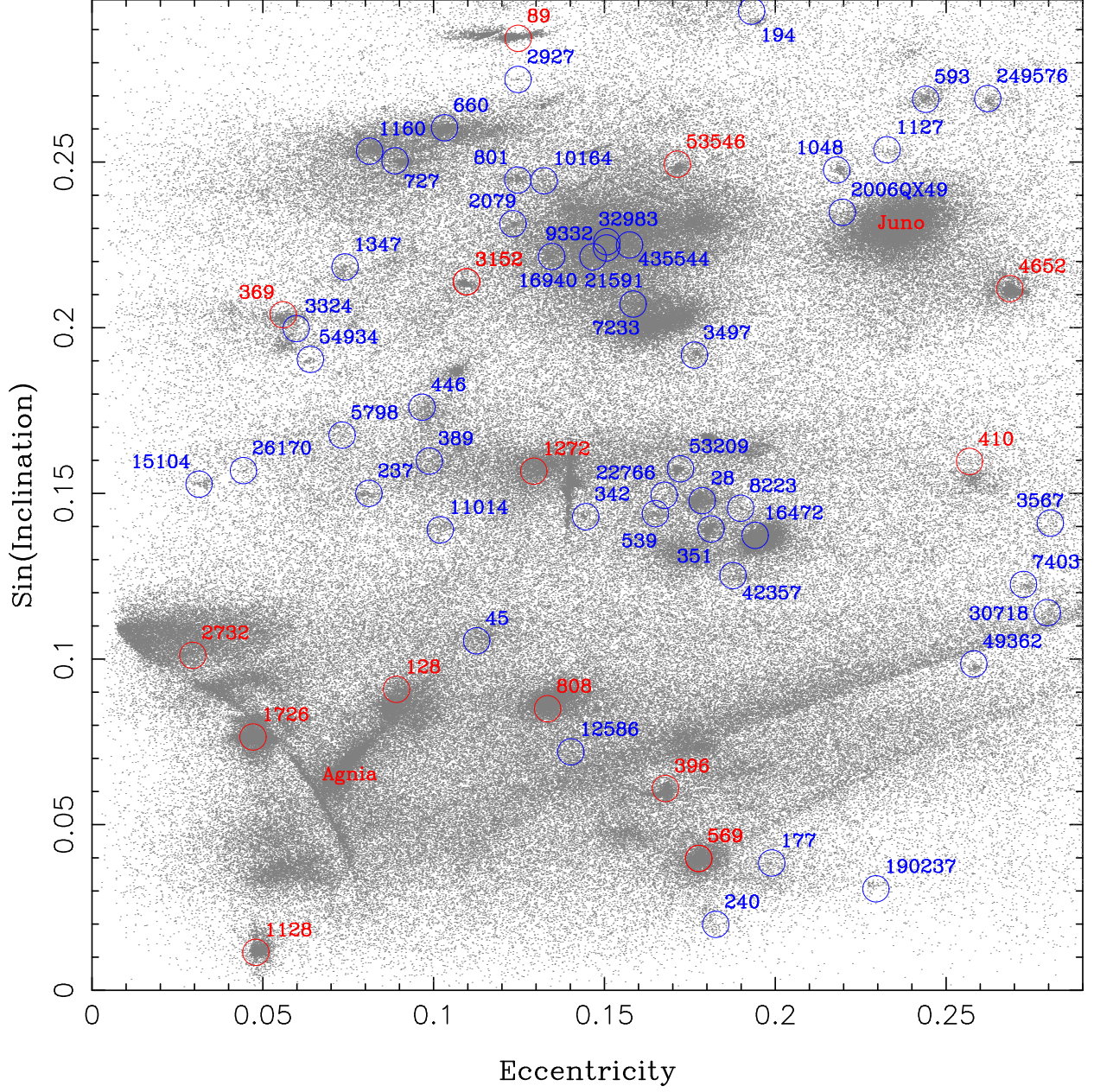


Fig. 6.— Proper eccentricities and sine of proper inclinations for middle belt asteroids ($2.5 < a_p < 2.825$ au). Notable families are labeled: blue labels stand for families identified in this work and not listed in Nesvorný et al. (2015), red labels are families known previously (not all previously known families are labeled).

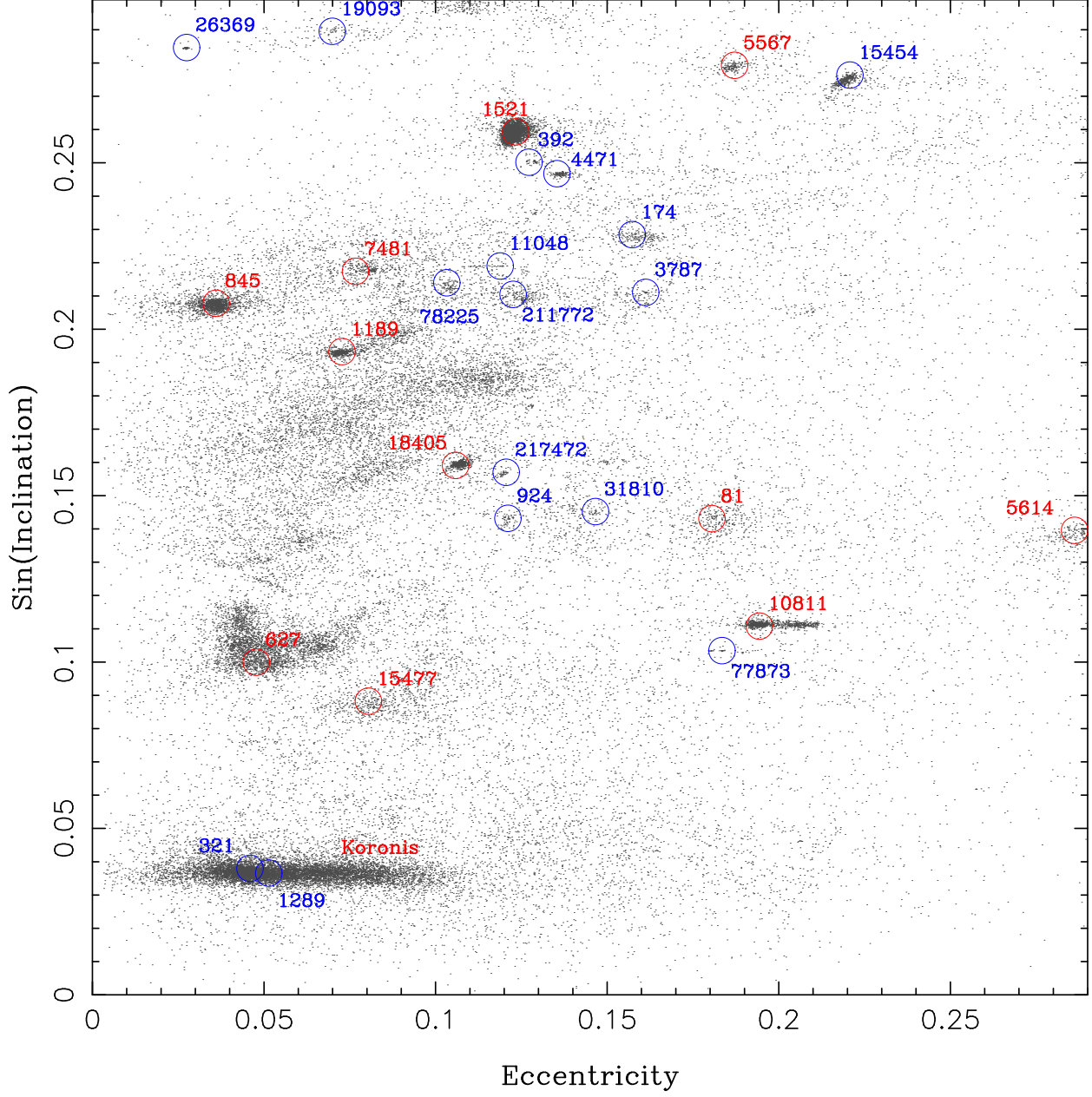


Fig. 7.— Proper eccentricities and sine of proper inclinations for asteroids in the pristine zone ($2.825 < a_p < 2.958$ au). Notable families are labeled: blue labels stand for families identified in this work and not listed in Nesvorný et al. (2015), red labels are families known previously (not all previously known families are labeled).

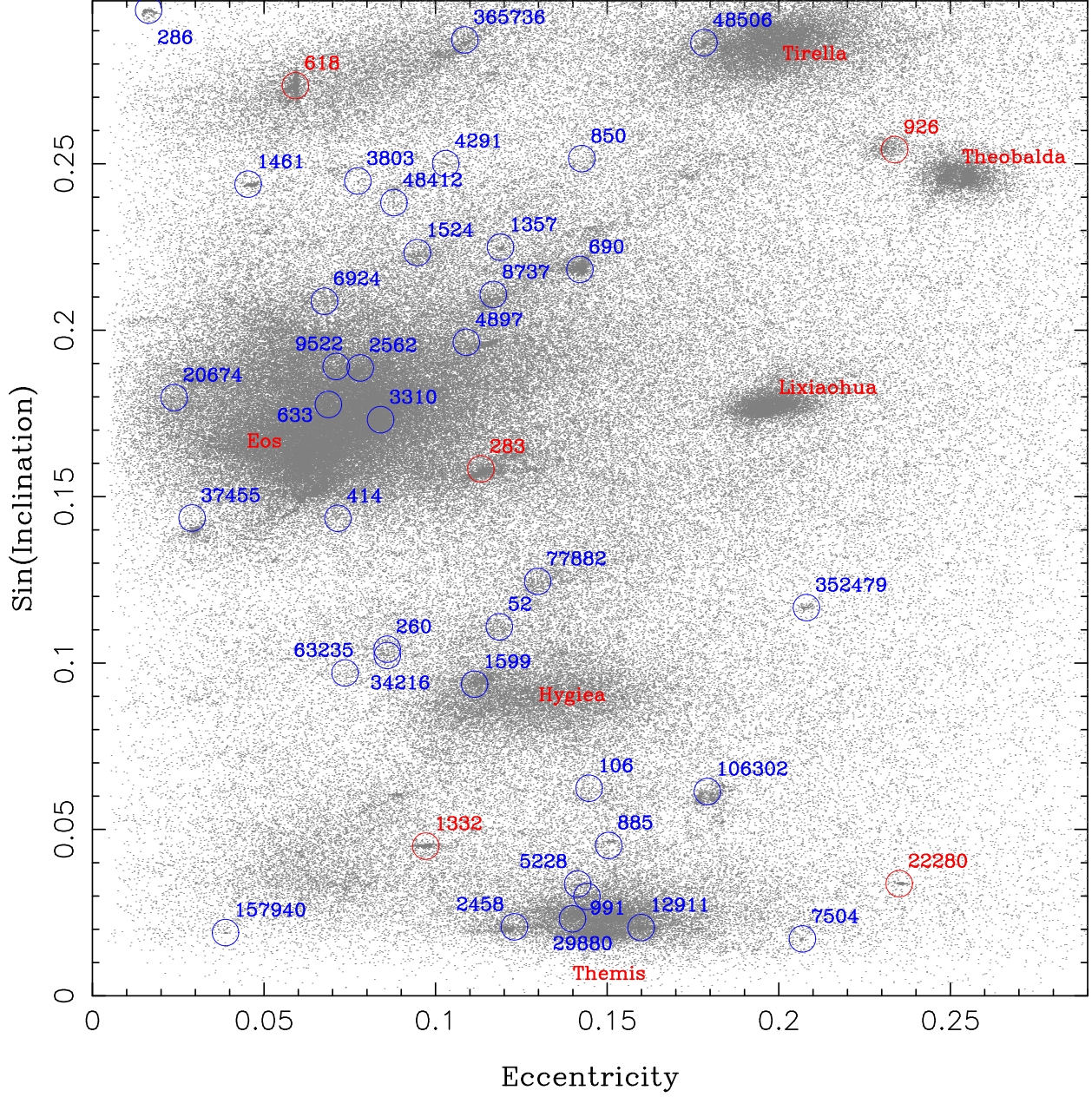


Fig. 8.— Proper eccentricities and sine of proper inclinations for outer belt asteroids ($2.958 < a_p < 3.8$ au). Notable families are labeled: blue labels stand for families identified in this work and not listed in Nesvorný et al. (2015), red labels are families known previously (not all previously known families are labeled).

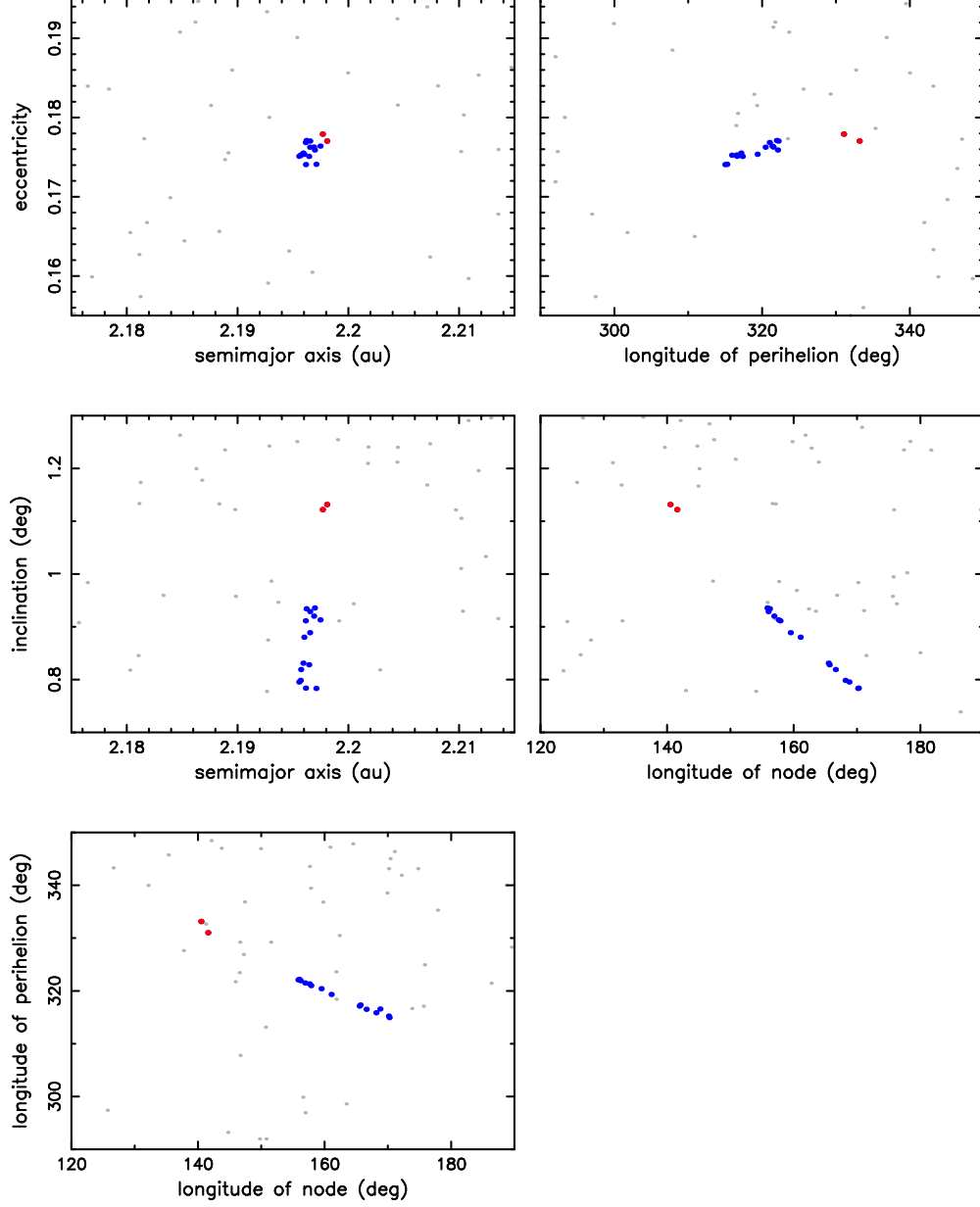


Fig. 9.— The osculating orbits of asteroids near the Moore-Sitterly family (MJD epoch 60400.0): (2110) Moore-Sitterly and (44612) 1999 RP27 are shown by red dots, other family members by blue dots; grey dots show background asteroids.

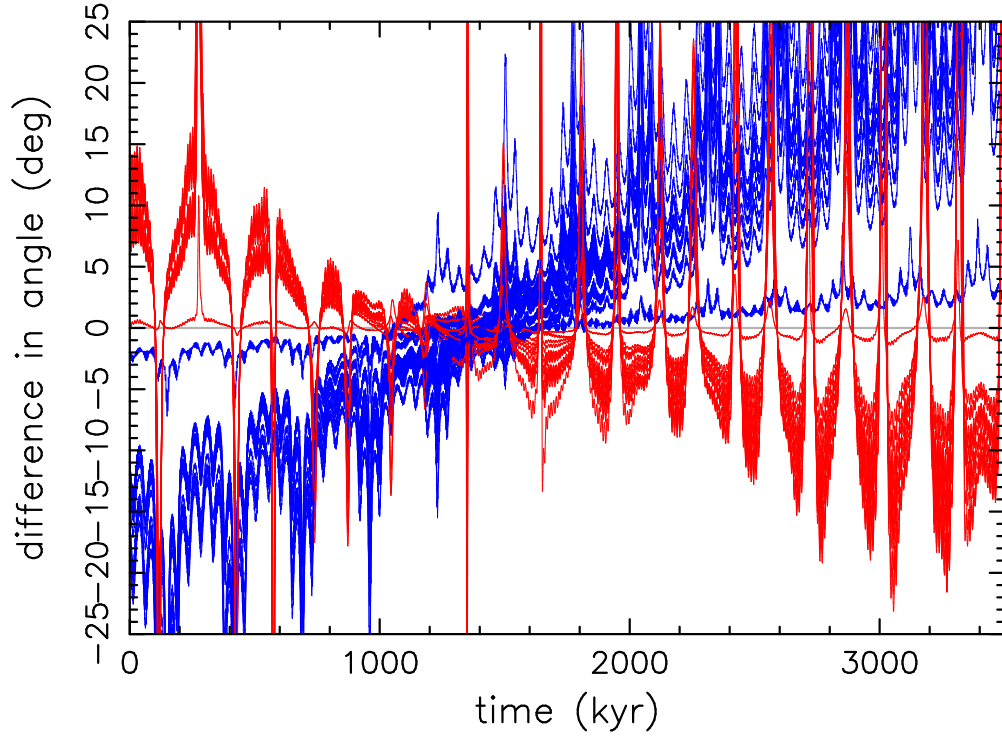


Fig. 10.— The past orbital convergence of secular angles 1.2-1.5 Myr ago indicates that the Moore-Sitterly family must be very young. The nodal longitudes are shown by red line, perihelion longitudes by blue. All 17 known family members are plotted here. Note that this result was obtained without considering the Yarkovsky acceleration in the N -body integrator. A careful analysis with the Yarkovsky force is left for future work.

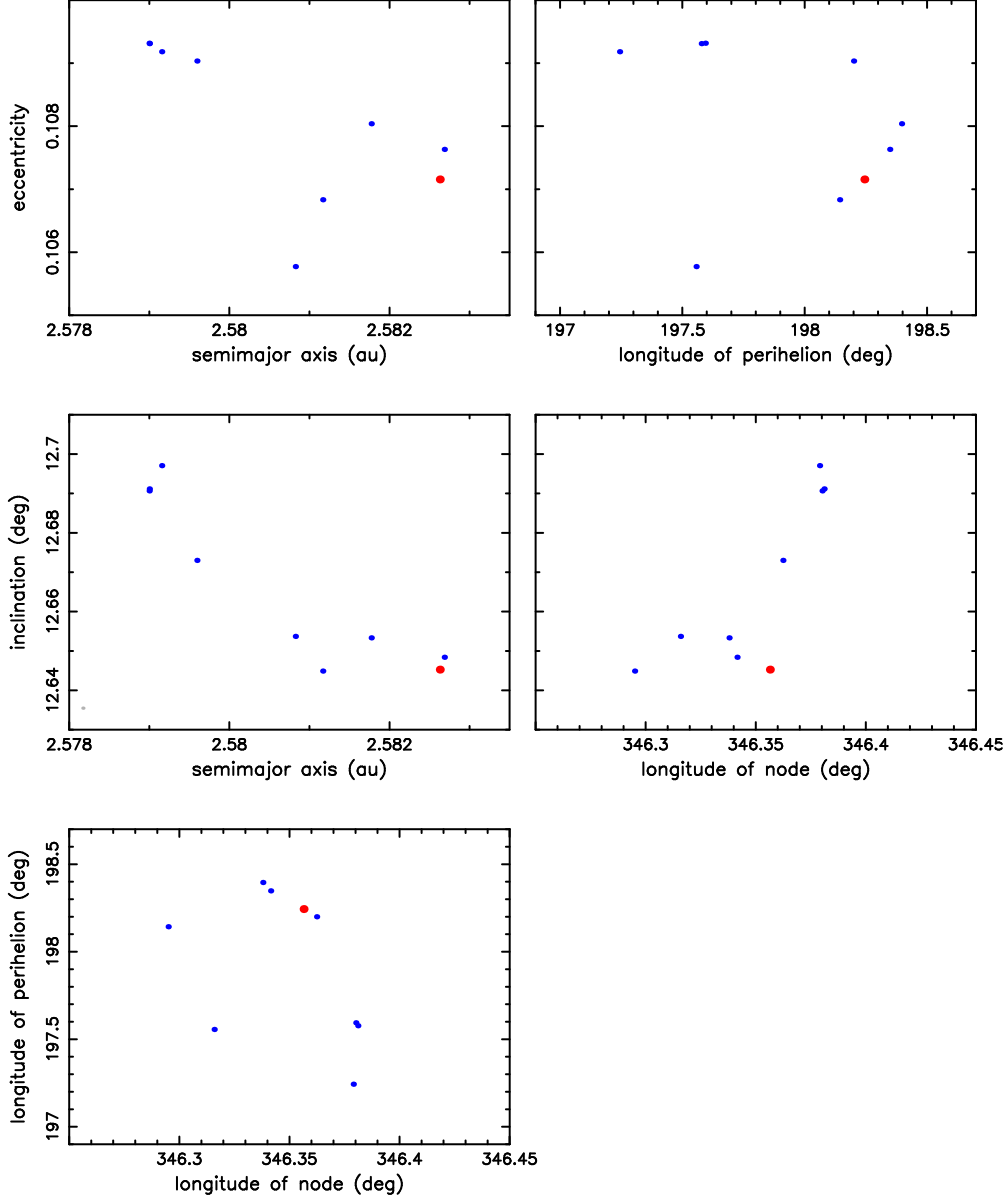


Fig. 11.— The osculating orbits of asteroids near the (9332) 1990SB1 family (MJD epoch 60400.0): the red dot is 9332, blue dots are small family fragments. The family is so compact that no background asteroids appear in any of these projections. Two family members, 2016DB45 and 2016EQ6, have practically identical orbits; the difference in the mean anomaly is only 0.6 deg. They appear as two overlapping dots in all projections.

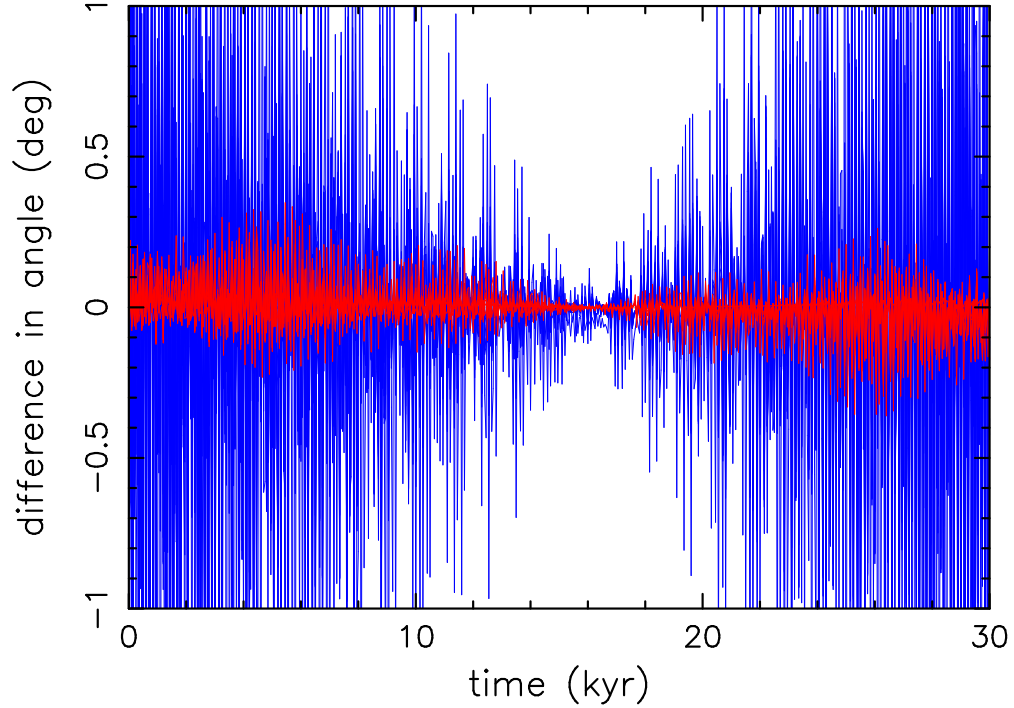


Fig. 12.— The past orbital convergence of secular angles 16-17 kyr ago indicates that the (9332) 1990SB1 family is extremely young. The nodal longitudes are shown by red lines, perihelion longitudes by blue. The mean anomalies of family members, not shown here, converge at 16-17 kyr ago as well. All 9 known family members are plotted here. This result was obtained without considering the Yarkovsky acceleration in the N -body integrator. A careful analysis with the Yarkovsky force is left for future work.

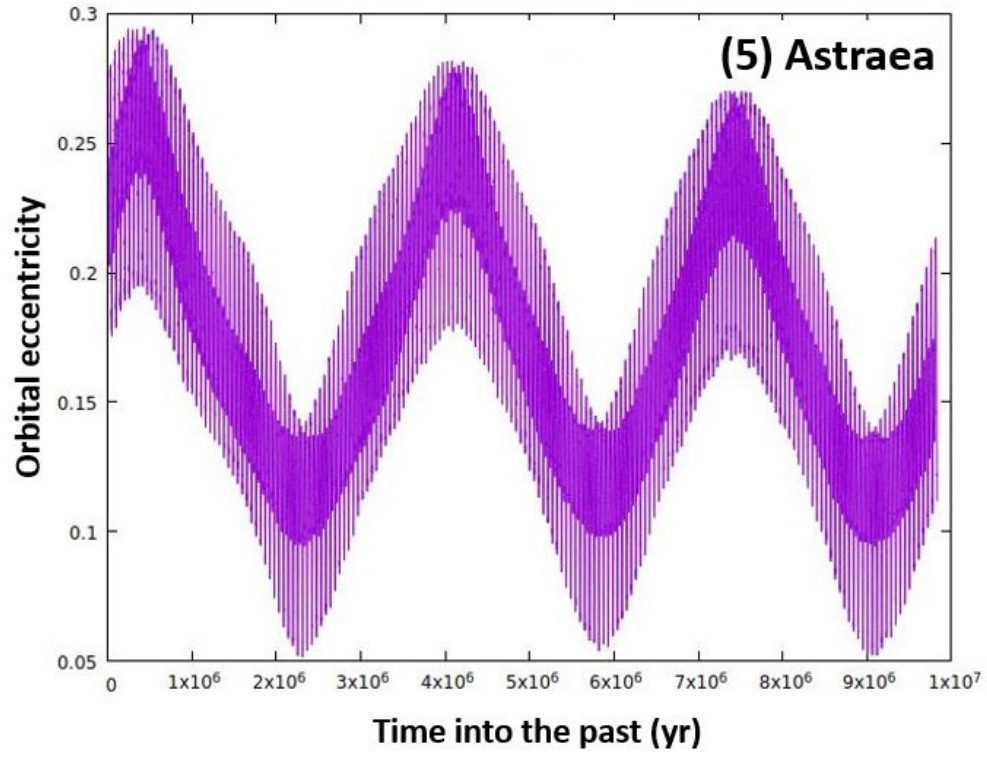


Fig. 13.— **Fig A1.** The orbital eccentricity of (5) Astraea shows large oscillations due to the interaction with the secular resonance $g + g_5 - 2g_6$.

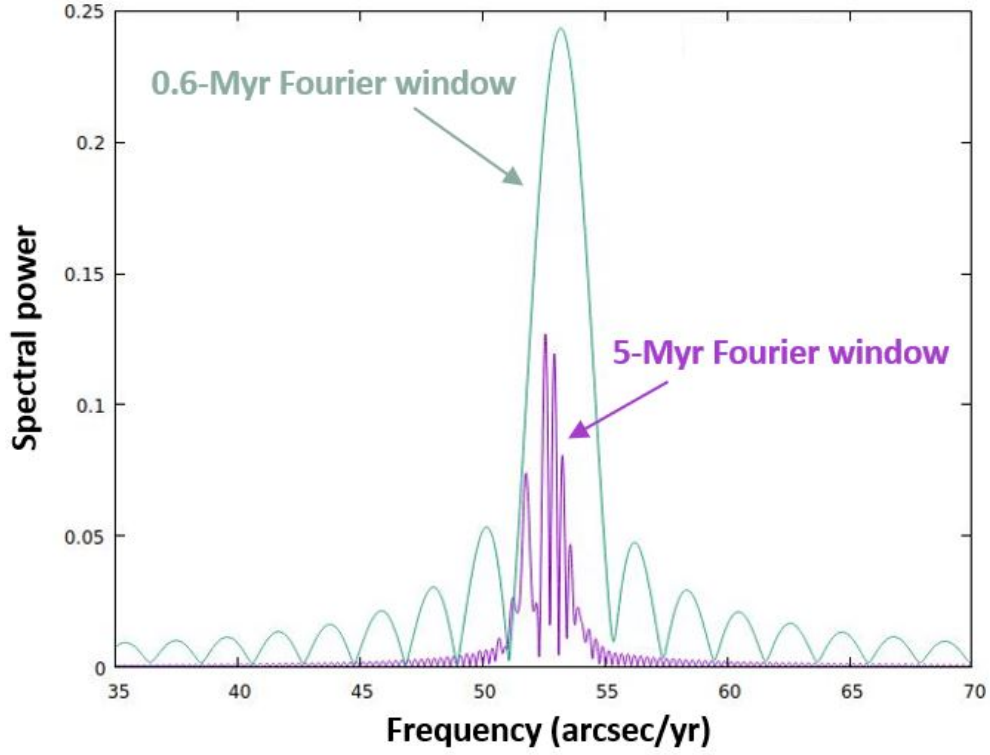


Fig. 14.— **Fig. A2** The Fourier spectrum of $e \cos(\varpi)$, $e \sin(\varpi)$ obtained for (5) Astraea from two different intervals: 0.6 Myr in green and 5 Myr in purple. The Fourier spectrum obtained from the 5-Myr long interval illustrates splitting of the proper frequency into several terms.